Note added 23/07/2019: We would like to advise readers that a Correction has been published on 22/07/2019 which affects Fig. S6, S7, S11 and S12 in this ESI document. This Correction can be found here: https://pubs.rsc.org/en/content/articlelanding/ta/2019/c9ta90156f (DOI: 10.1039/C9TA90156F).

Supplementary Materials For

Bottom-up Synthesis of Fully sp^2 Hybridized Three-dimensional Microporous Graphitic Frameworks as Metal-free Catalysts

Siddulu Naidu Talapaneni,[a,†] Jaehoon Kim,[a,†] Sang Hyun Je,[a] Onur Buyukcakir,[a] Jihun Oh[a]* and Ali Coskun[a,b]*

[a]Graduate School of EEWS and KAIST Institute NanoCentury, Korea Advanced Institute of Science and Technology (KAIST), 291 Daehak-ro, Yuseong-gu, Daejeon 34141, Republic of Korea

[b]Department of Chemistry, Korea Advanced Institute of Science and Technology (KAIST), 291 Daehak-ro, Yuseong-gu, Daejeon 34141, Republic of Korea

Email: jihun.oh@kaist.ac.kr, coskun@kaist.ac.kr

[†] These authors contributed equally to this work.

Electronic Supplementary Information (ESI)

Contents:

Section 1. Materials and characterization methods **S3-S4**

Section 2. Experimental procedures for the synthesis of 2D- and 3D-MGFs **S4**

Section 3. Synthesis and characterization of octaketotetraphenylene **S5-S10**

Section 4. Synthesis and characterization of hexaketotriphenylene **S10-S13**

Section 5. Characterization of 2D and 3D-MGFs **S14-S28**

Section 6. Electrochemical characterization of 2D and 3D-MGFs **S29-S30**

Section 7. References **S30**

1. Materials and Characterization methods

All manipulations involving air- and/or moisture-sensitive compounds were carried out using a glove box or standard Schlenk line techniques under Ar atmosphere. Air-sensitive liquids were transferred *via* syringe and addition funnels and were injected into the reaction flask through rubber septa. Moisture sensitive solids were transferred in a dry glovebox under Ar atmosphere. Analytical thin-layer chromatography was performed using silica gel pre-coated on aluminum sheets. Visualization of developed chromatograms was performed by exposure to UV or iodine vapor. Flash column chromatography was carried out using 230-400 mesh silica. All chemicals and solvents were purchased from Sigma-Aldrich and used without further purification. The ^{1}H NMR spectra were recorded on a Bruker DMX 300 MHz and ^{13}C NMR spectra were obtained using Bruker Avance 400 MHz NMR instrument. Chemical shifts in ^{1}H NMR spectra are reported in parts per million (ppm) from tetramethylsilane, with the solvent resonance used as an internal standard. Data are presented in the following order: chemical shift, multiplicity (*s* = singlet, *d* = doublet, *t* = triplet, *q* = quartet, *qn* = quintet, *sx* = sextet, *h* = heptet, *o* = octet, *m* = multiplet, and *br* = broad), coupling constant in *Hz*, and integration. Chemical shifts for ^{13}C NMR spectra are reported in parts per million (ppm) from tetramethylsilane, using the central peak of the solvent resonance as the internal standard.

The powder X-ray diffraction (XRD) patterns of MGFs were collected on a Rigaku D/MAX-2500 (18 kW) micro area X-ray diffractometer using CuKα (*k* = 0.154 nm) radiation. The X-ray diffractograms were recorded in the 2θ range of 5–70^{o} with a 2θ step size of 0.15 and a step time of 1 s. The morphology of MGFs were investigated using a field emission scanning electron microscope (FE-SEM, Sirion). High resolution transmission electron microscopy (HRTEM, TECNAI) and energy-dispersive X-ray analyses (EDAX) were used for microstructure characterization and elemental mapping, respectively. Detailed characters of various chemical bonds in each sample were characterized by Raman spectroscopy (Horiba Jobin Yvon) equipped with a 633 nm wavelength He-Ne laser as well as Fourier-transform infrared spectroscopy (FTIR, Bruker) by preparing KBr pellets. X-ray photoelectron spectroscopy (XPS) analysis was performed with a multi-purpose XPS (Sigma Probe, Thermo VG Scientific, X-ray Source: monochromatic Al K(alpha)). The carbon, nitrogen and hydrogen of NGR samples were investigated using an element analyzer (FlashEA 2000 (Series) [C, H, N] Elemental Analyzer). The Ar adsorption and desorption isotherms were measured at 87 K on a Micrometrics 3Flex Surface Characterization Analyzer. All samples were outgassed at 200^{o}C for 6 h prior to the analysis.

Electrochemical characterization: Electrochemical properties of 2D and 3D nitrogenated microporous graphitic frameworks (MGFs) were characterized in a typical three-electrode system using an SP-150 potentiostat (Bio-Logic, USA). A Ag/AgCl (3M NaCl) and a graphite rod were used as a reference electrode (RE) and a counter electrode (CE), respectively. Pt/C catalyst (20% Pt on Vulcan XC-72) and a glassy carbon electrode (GCE, 3 mm in diameter) were used for comparison. Catalytic inks of 2D- and 3D-MGFs were prepared as following: 8 mg of the synthesized 2D and 3D-MGF was added in a mixed solution of 80 µl of 5 wt% Nafion 117 solution (Sigma-Aldrich) and 1 mL of H_2O/EtOH (80% v/v), followed by sonication for 1 h for homogenous dispersion. In order to measure the electrocatalytic activities of the catalysts, 5 µL of

the mixed catalytic inks were dropped onto the GCE (i.e., loading amount of 0.566 mg cm^{-2}) and dried under ambient conditions for overnight. All experiments were conducted in 0.5 M H_2SO_4 purged with ultrapure Ar gas (99.999 %) for 15 min to remove dissolved oxygen before measurements. All polarization curves (J-V) were compensated by iR-correction and recorded with the scan rate of 5 mV s^{-1} toward cathodic direction. Every current density was normalized with respect to the apparent surface area of the GCE (ca. 0.071 cm^2). In addition, all potentials were expressed as reversible hydrogen electrode (RHE) by $E_{RHE} = E_{WE} + (0.209 + 0.059 * pH)$ V. The electrochemical impedance spectroscopy (EIS) was carried out, collected at the applied potential of -0.40 V (vs. RHE) from 10^5 to 0.1 Hz.

The improved electrocatalytic activity of 2D and 3D-MGFs was achieved by simply immersion into 0.5 M H_2SO_4 solution. We denoted such acid treated 2D and 3D-MGFs, as H^+-2D-MGF and H^+-3D-MGF, respectively. Meanwhile, in order to find the optimal immersion time, we have investigated the electrocatalytic activities of H^+-2D-MGF and H^+-3D-MGF with different immersion times using linear sweep voltammetry (LSV). As a result, we observed that the electrocatalytic activities of both 2D- and 3D-MGFs were gradually improved up to 6 days immersion, and afterwards, it became nearly saturated. Therefore, we performed all experiments with H^+-2D- and H^+-3D-MGFs which were immersed in 0.5 M H_2SO_4 solution for 6 days, unless otherwise stated.

2. Experimental procedures for the synthesis of MGFs

3D-MGF: 1,2,4,5-Benzenetetramine tetrahydrochloride (28.4 mg, 0.1 mmol), octaketotetraphenylene (21.0 mg, 0.05 mmol) and $ZnCl_2$ (137 mg, 1.0 mmol) were mixed in a 10 mL pyrex ampoule. The ampoule was evacuated under vacuum, sealed and heated at the designated temperatures (350, 400 and 450ºC) for 15 h with 3ºC min^{-1} ramping. The ampule was cooled down to room temperature and the resulting black tablet was grounded in a mortar, washed thoroughly with aq. HCl solution (1 M) to remove the $ZnCl_2$ residues, further rinsed with H_2O, MeOH, and THF, filtered and dried under vacuum at room temperature for 24 h, to give 3D-MGF as a black powder with the isolated yields of 75-80%.

2D-MGF: 1,2,4,5-Benzenetetramine tetrahydrochloride (21.3 mg, 0.075 mmol), hexaketotriphenylene (16.0 mg, 0.05) and $ZnCl_2$ (103 mg, 0.75 mmol) were mixed in a 10 mL pyrex ampoule. The ampoule was evacuated under vacuum, sealed and heated at the designated temperatures (350, 400 and 450ºC) for 15 h with 3ºC min^{-1} ramping. The ampule was cooled down to room temperature and the resulting black tablet was ground in a mortar, washed thoroughly with aq. HCl solution (1 M) to remove the $ZnCl_2$ residues, further rinsed with H_2O, MeOH, and THF, filtered and dried under vacuum at room temperature for 24 h, to give 2D-MGFs as black powder with the isolated yields of 81-85%.

3. Synthesis and characterization of octaketotetraphenylene

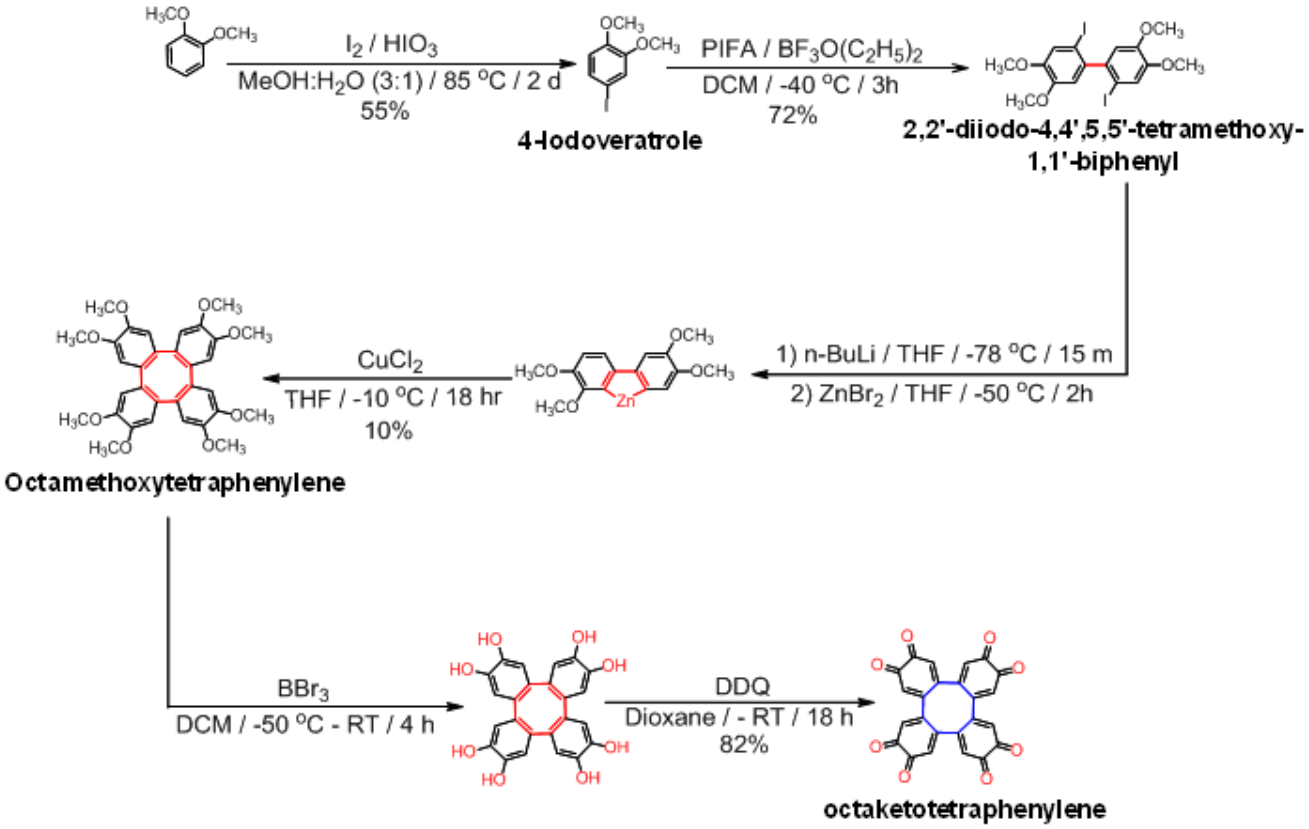

Figure S1. Synthetic scheme for the preparation of octaketotetraphenylene.

Synthesis of 4-iodoveratrole.[1, 2] A 1 L round-bottom flask was charged with veratrole (10.36 g, 75.0 mmol), I_2 (4.75g, 37.5 mmol) and iodic acid, HIO_3, (2. 63 g, 15.0 mmol) in 3:1 ratio of MeOH:H_2O (750 mL). The mixture was stirred at 85°C for 48 h, yielding a dark colored suspension. After complete consumption of the starting material, the solvent was removed under reduced pressure. The obtained crude product was diluted with CH_2Cl_2 and washed with aq. sodium thiosulfate solution (5 wt% $Na_2S_2O_3$) and subsequently with brine solution. Organic layers were separated, dried over Na_2SO_4 and concentrated under reduced pressure. Dark colored thick oily liquid was purified by Kugelrohr distillation apparatus at 100ºC under vacuum to yield reddish colored 4-iodoveratrole (10.89 g, 55%). ^{1}H NMR (300 MHz, $CDCl_3$) = δ 7.40 – 7.25 (*m*, 2H), 6.74 (*d*, *J* = 9.0 Hz, 1H), 4.00 (*s*, 3H), 3.99 (*s*, 3H) ppm.

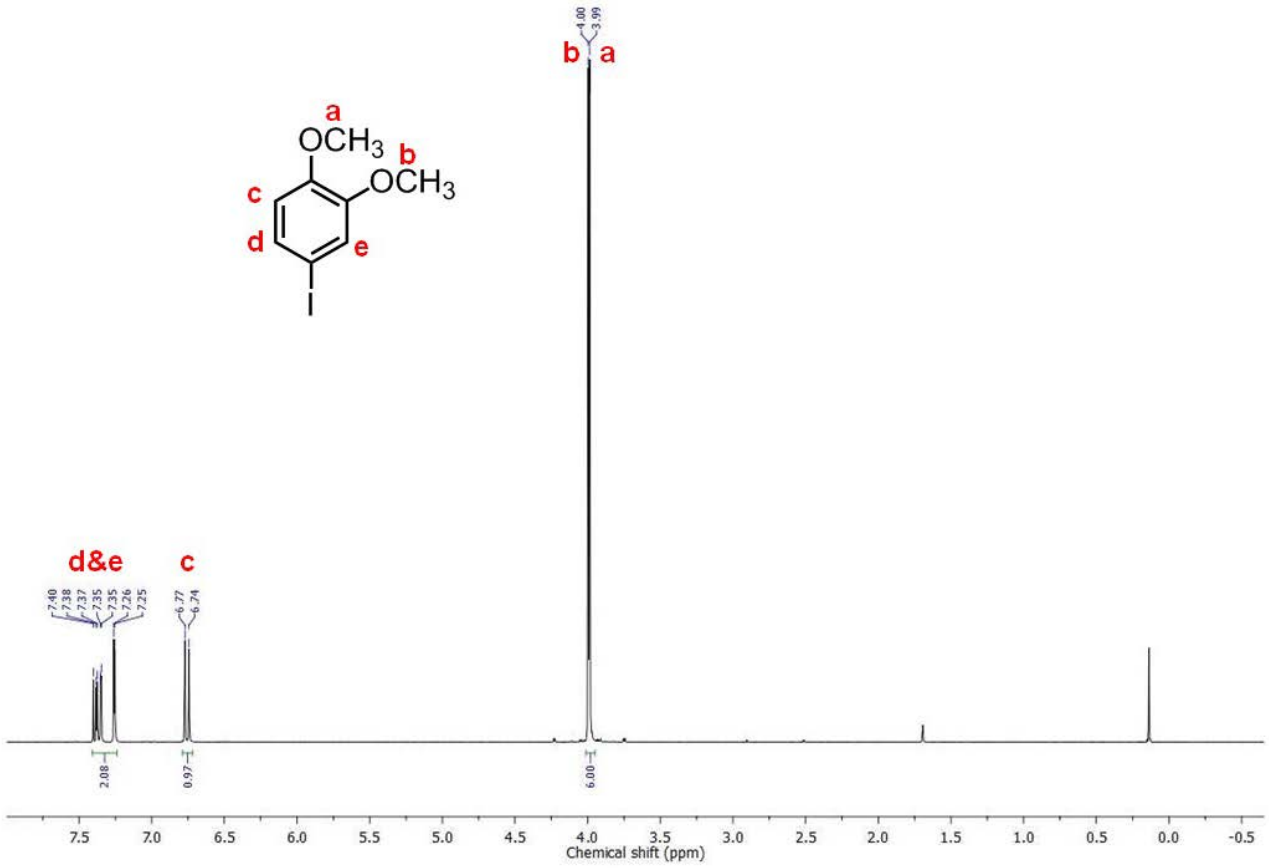

Figure S2. ^{1}H NMR (300 MHz, $CDCl_3$, 298 K) spectrum of 4-iodoveratrole.

Synthesis of 2,2'-diiodo-4,4',5,5'-tetramethoxy-1,1'-biphenyl.[3, 4] 4-Iodoveratrole (4.0 g, 15.14 mmol, 1.00 equiv.) was dissolved in CH_2Cl_2 (100 mL) in a 500 mL round-bottomed flask and cooled to -78ºC. To this solution. a pre-mixed solution of [bis(trifluoroacetoxy)iodo]benzene, PIFA, (3.58 g, 8.33 mmol, 0.55 equiv.) and $BF_3.Et_2O$ (2.05 mL, 16.62 mmol, 1.10 equiv.) in CH_2Cl_2 (50 mL) was added dropwise over 1 h. The reaction mixture was stirred until the starting material was completely consumed (~ 2 h). The reaction was quenched by adding 10% NaOH solution (100 mL) and the reaction mixture was vigorously stirred for 1 h. The product was extracted with CH_2Cl_2 (3 x 100 mL). The combined organic layers were dried over Na_2SO_4 and concentrated under vacuum. The crude product was subjected to silica gel column chromatography with 10% EtOAc:Hexane as the mobile phase. Concentrated column fractions were allowed to crystalize to yield reddish off white colored compound of 2,2'-diiodo-4,4',5,5'-tetramethoxy-1,1'-biphenyl (5.7 g, 72%). ^{1}H NMR (300 MHz, $CDCl_3$) = δ 7.31 (*s*, 1H), 6.73 (*s*, 1H), 3.92 (*s*, 3H), 3.86 (*s*, 3H) ppm.

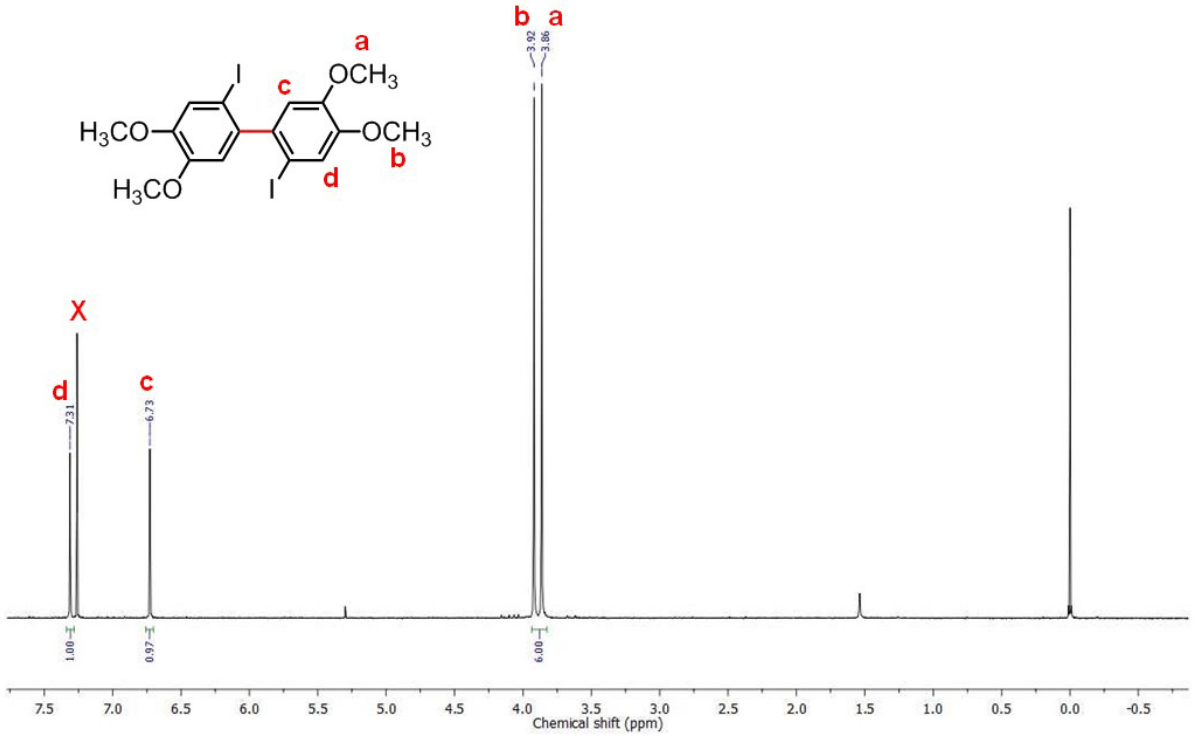

Figure S3. ^{1}H NMR (300 MHz, $CDCl_3$, 298 K) spectrum of 2,2'-diiodo-4,4',5,5'-tetramethoxy-1,1'-biphenyl.

Synthesis of Octamethoxytetraphenylene.[5-7] To a cooled solution of 2,2'-diiodo-4,4',5,5'-tetramethoxy-1,1'-biphenyl (4.0 g, 7.6 mmol) in 200 mL of THF was dropwise added *n*-BuLi (10.4 mL, 16.73 mmol, 1.6 M in hexanes) at -78ºC for 15 min and the resulting mixture was stirred for 15 min. Then the temperature was raised to -50ºC and a solution of $ZnBr_2$ (2.06 g, 9.13 mmol) in 50 mL THF was dropwise added over 15 min and the stirring was continued for additional 2 h at -50ºC. After cooling the reaction mixture to -78 ºC, $CuCl_2$ (3.064 g, 22.8 mmol) was added. The resulting mixture was allowed to warm to room temperature and the stirring was continued for 18 h. The mixture was filtered over SiO_2, washed with EtOAc (100 mL) and the combined organic layers were concentrated. The residue was diluted with CH_2Cl_2 (200 mL), washed with brine (500 mL), dried over Na_2SO_4 and finally evaporated under reduced pressure. The crude product was subjected to silica gel column chromatography with three phase solvent system of 25% EtOAc/CH_2Cl_2/Hexane as the mobile phase. Concentrated column fractions were allowed to recrystallized from iPr$_2$O/CH_2Cl_2 to yield reddish colored compound of octamethoxytetraphenylene (0.4 g, 10%). ^{1}H NMR (300 MHz, $CDCl_3$) = 6.70 (*s*, 1H), 3.86 (*s*, 3H) ppm. ^{13}C NMR (100 MHz, $CDCl_3$) = δ 150.5, 136.7, 115.1, 58.6 ppm. MALDI-TOF-MS for $C_{32}H_{32}O_8$ (calculated: 544.6), found: 544.3 ([M]$^+$).

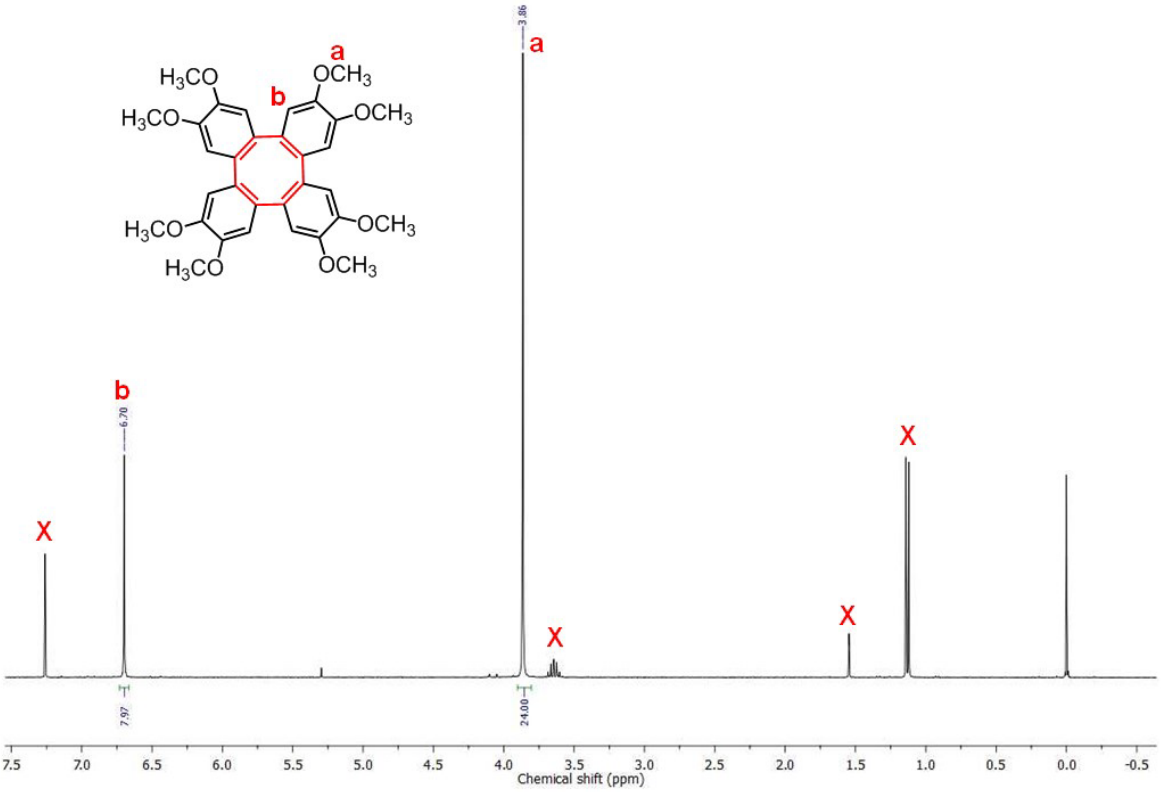

Figure S4. ^{1}H NMR (300 MHz, $CDCl_3$, 298 K) spectrum of octamethoxytetraphenylene.

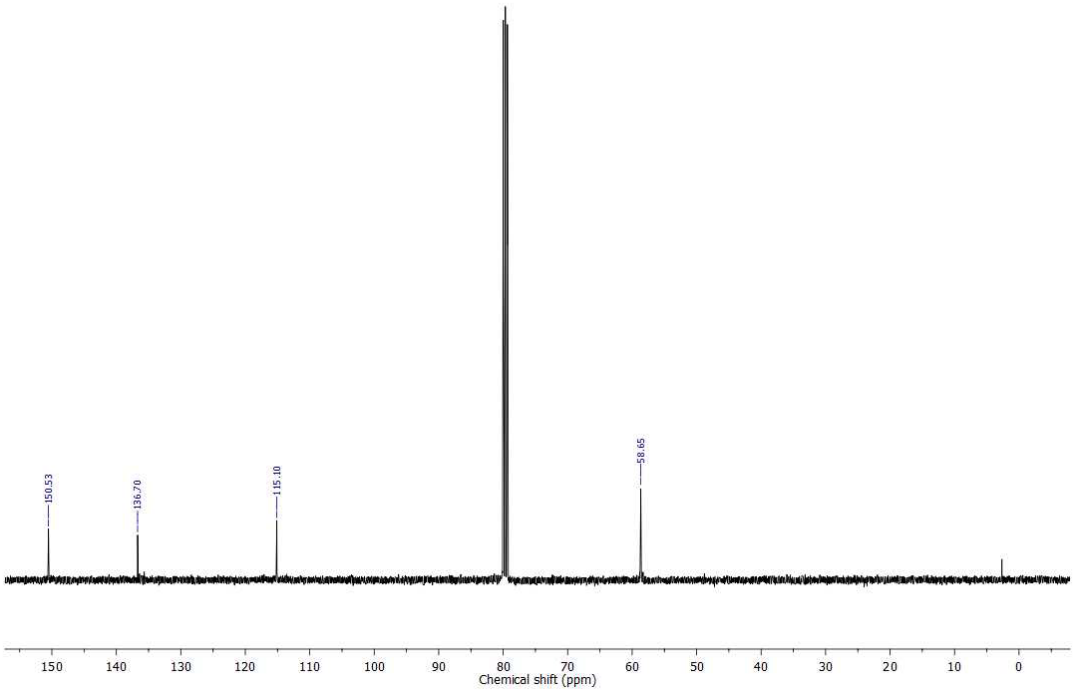

Figure S5. ^{13}C NMR (100 MHz, $CDCl_3$, 298 K) spectrum of octamethoxytetraphenylene.

Synthesis of octaketotetraphenylene. Octamethoxytetraphenylene (0.27 g, 0.50 mmol) in 2.0 mL of CH_2Cl_2 was treated with 4.2 mL (4.2 mmol) BBr_3 (1M solution in CH_2Cl_2) at -50ºC and stirred at same temperature for 1 h. The resulting mixture was stirred for additional 3 h at room temperature. The solvent was removed under vacuum and the residue was dissolved in degassed MeOH and stirred for 2 h. The solvent was removed and the residue was redissolved in 5 mL of dioxane and treated with 2,3-dichloro-5,6-dicyano-1,4-benzoquinone (DDQ: 0.115 g, 0.5 mmol) for 16 h at room temperature and filtered off, concentration of filtrate under reduced pressure afforded octaketotetraphenylene dark grey colored solid (0.17 g, 82%). ^{1}H NMR (300 MHz, DMSO-d_6) = 6.36 (*s*, 1H) ppm. ^{13}C NMR (100 MHz, $CDCl_3$) = δ 151.2, 120.5, 102.0, 72.3, 66.7 ppm ESI-HRMS calcd for *m/z* = 425.0292 $[M - H]^+$, found *m/z* = 425.0231.

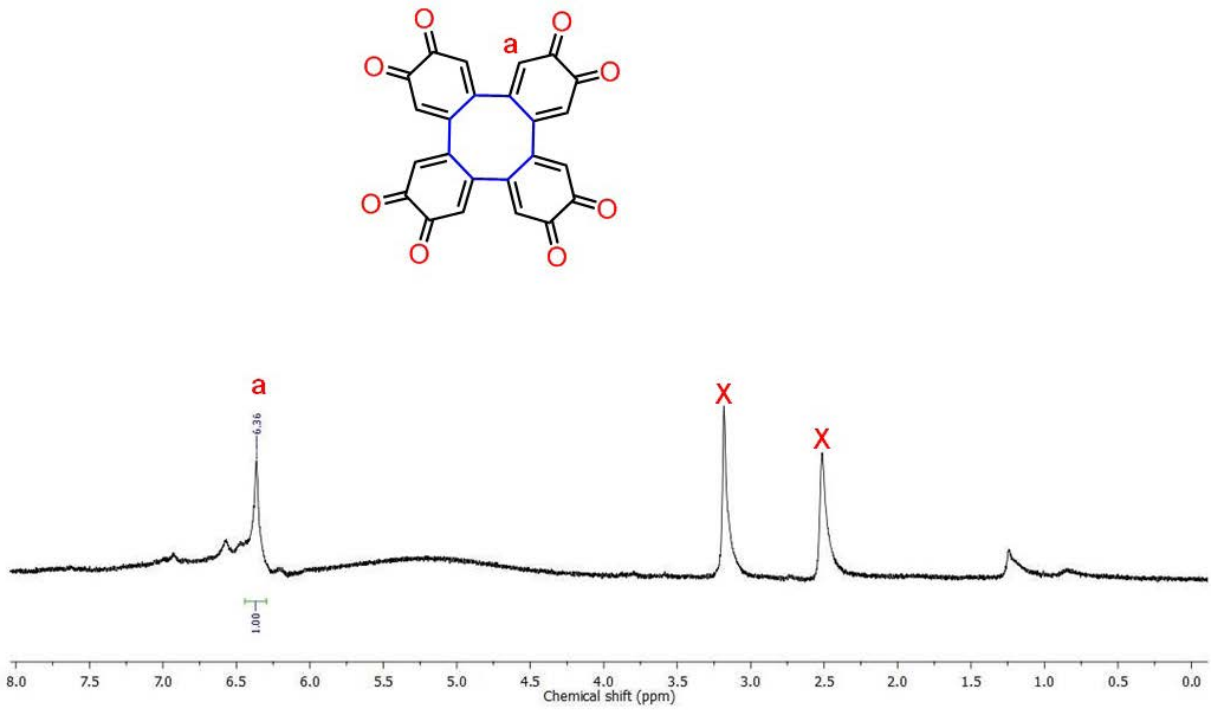

Figure S6. ^{1}H NMR (300 MHz, DMSO-d_6, 298 K) spectrum of octaketotetraphenylene.

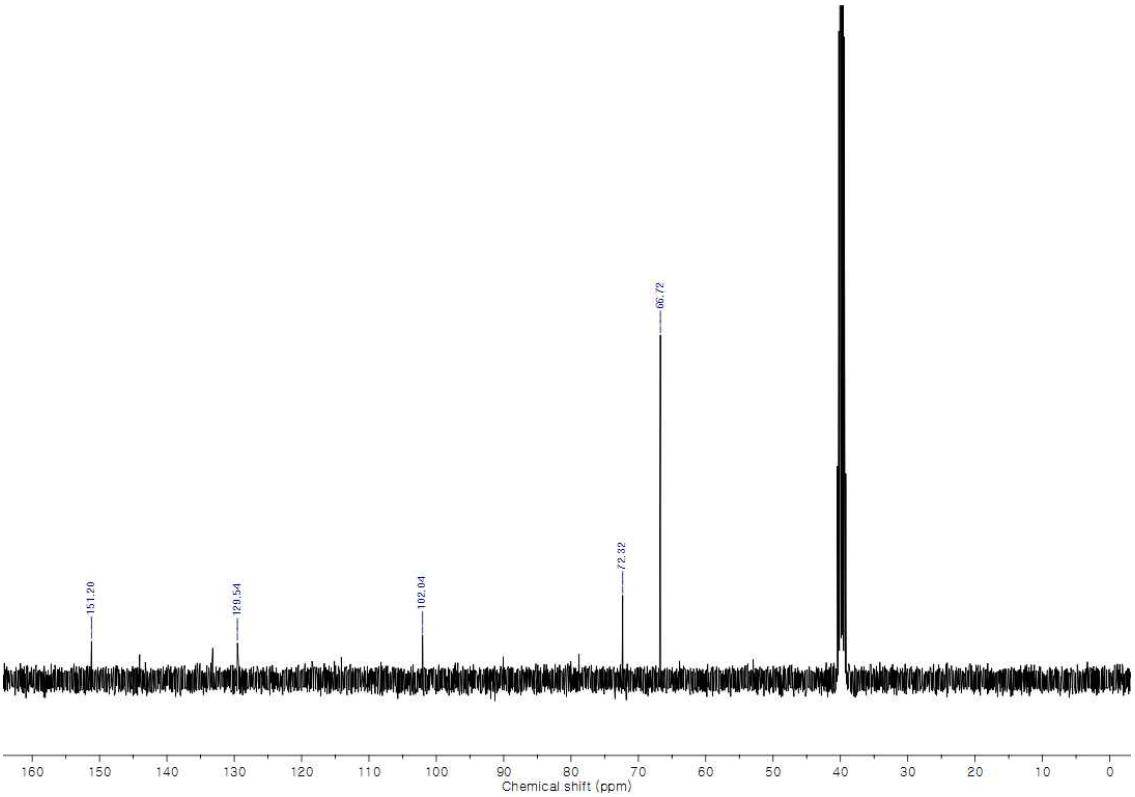

Figure S7. ^{13}C NMR (100 MHz, DMSO-d_6, 298 K) spectrum of octaketotetraphenylene.

4. Synthesis and characterization of hexaketotriphenylene

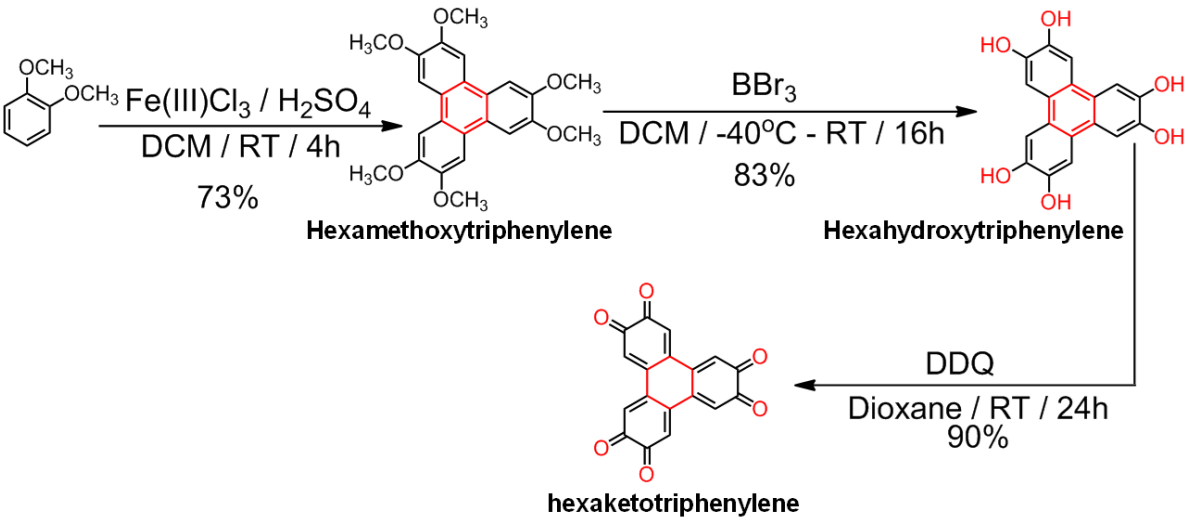

Figure S8. Synthetic scheme for the preparation of hexaketotriphenylene.

Synthesis of hexamethoxytriphenylene.[8] A solution of Veratrol (13.82 g, 100 mmol) in CH_2Cl_2 (140 mL) was added dropwise to a suspension of $FeCl_3$. xH_2O (53 g) in CH_2Cl_2 (300 mL) and concentrated H_2SO_4 (0.7 mL). After the complete addition over 15 min, the reaction mixture was further stirred for 4 h at room temperature, then 400 mL of MeOH were slowly added under vigorous stirring. The obtained mixture was stirred for additional 30 min and the precipitate was filtered off, washed with MeOH (5 x 100 mL) and dried under vacuum to give hexamethoxytriphenylene as a slightly beige powder (10.1 g, 83%). ^{1}H NMR (300 MHz, $CDCl_3$) = 7.81 (*s*, 1H), 4.13 (*s*, 3H) ppm.

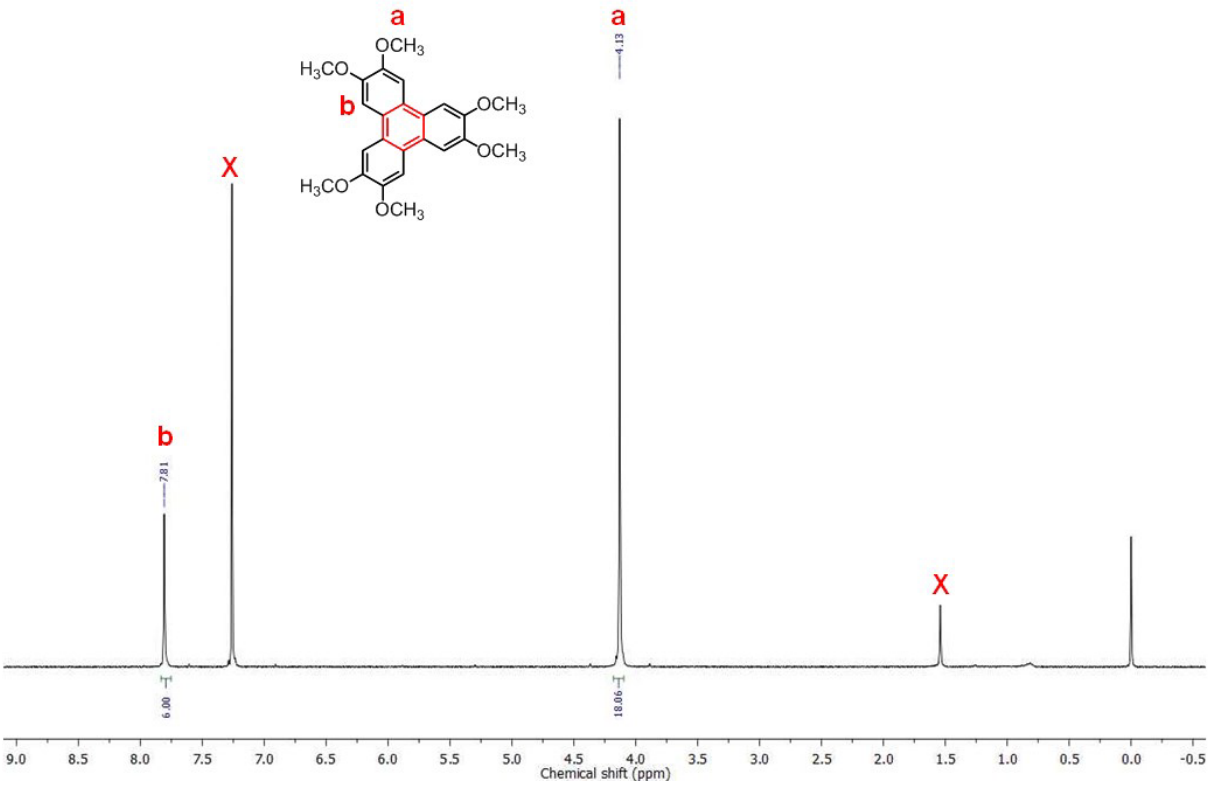

Figure S9. ^{1}H NMR (300 MHz, $CDCl_3$, 298 K) spectrum of hexamethoxytriphenylene.

Synthesis of hexahydroxytriphenylene.[8] Hexamethoxytriphenylene (1.02 g, 2.5 mmol) was dissolved in CH_2Cl_2 (20 mL) and the resulting solution was cooled to -70ºC and kept at this temperature under a N_2 atmosphere. A solution of BBr_3 (1 M in CH_2Cl_2, 30 mL) was then added dropwise to the reaction mixture over a period of 30 min. After the complete addition, the reaction temperature was gradually allowed to reach room temperature and stirring was continued for 16 h. The reaction mixture was then slowly poured into crushed ice (100 g) and the obtained mixture was stirred vigorously until all the ice melted. It was then extracted with Et_2O (6 x 150 mL) and the combined organic extracts were washed with brine solution, dried over Na_2SO_4 and concentrated under vacumm. This afforded hexahydroxytriphenylene as a grey solid (0.7 g, 83%). ^{1}H NMR (300 MHz, Acetone-d_6) = 8.23 (*s*, 3H), 7.83 (*s*, 6H) ppm.

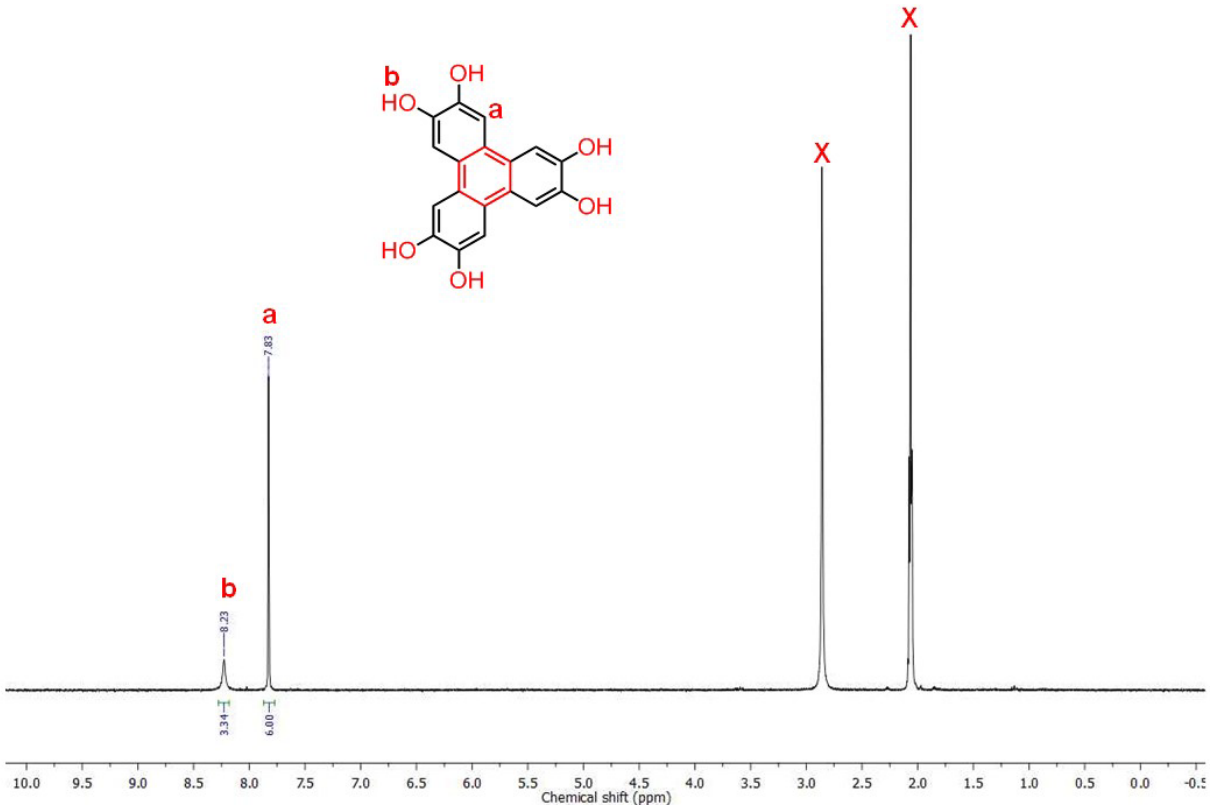

Figure S10. ^{1}H NMR (300 MHz, Acetone-d_6, 298 K) spectrum of hexahydroxytriphenylene.

Synthesis of hexaketotriphenylene. The hexahydroxytriphenylene (0.4 g, 1.22 mmol) was dissolved in 10 mL of Dioxane and treated with 2,3-dichloro-5,6-dicyano-1,4-benzoquinone (DDQ: 0.288 g, 1.26 mmol) for 24 h at room temperature and filtered off, concentration of filtrate under reduced pressure afforded hexaketotriphenylene as a dark grey colored solid in a quantitative yield. ^{1}H NMR (300 MHz, DMSO-d_6) = 8.32 (*s*, 1H) ppm. ^{13}C NMR (100 MHz, $CDCl_3$) = δ 151.2, 129.5, 114.0, 102.0, 72.3 ppm ESI-MS calcd for *m/z* = 360.0503 [*M* – MeCN – H]$^{+}$, found *m/z* = 360.0527.

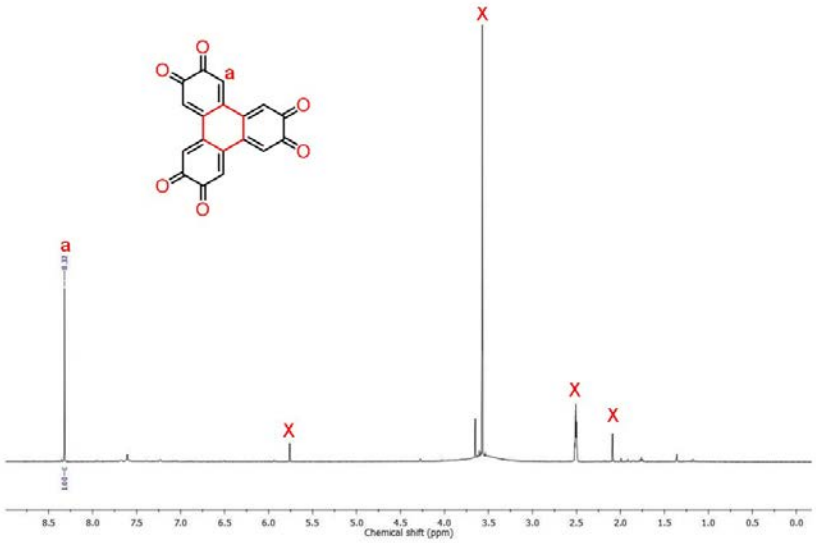

Figure S11. ^{1}H NMR (300 MHz, DMSO-d_6, 298 K) spectrum of hexaketotriphenylene.

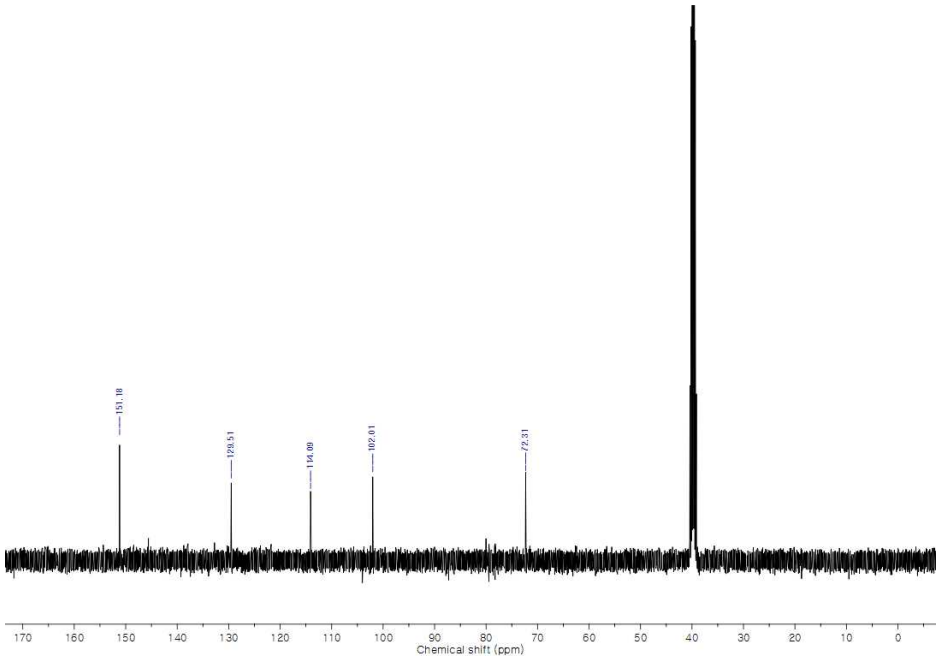

Figure S12. ^{13}C NMR (100 MHz, DMSO-d_6, 298 K) spectrum of hexaketotriphenylene.

5. Characterizations of 2D and 3D-MGFs

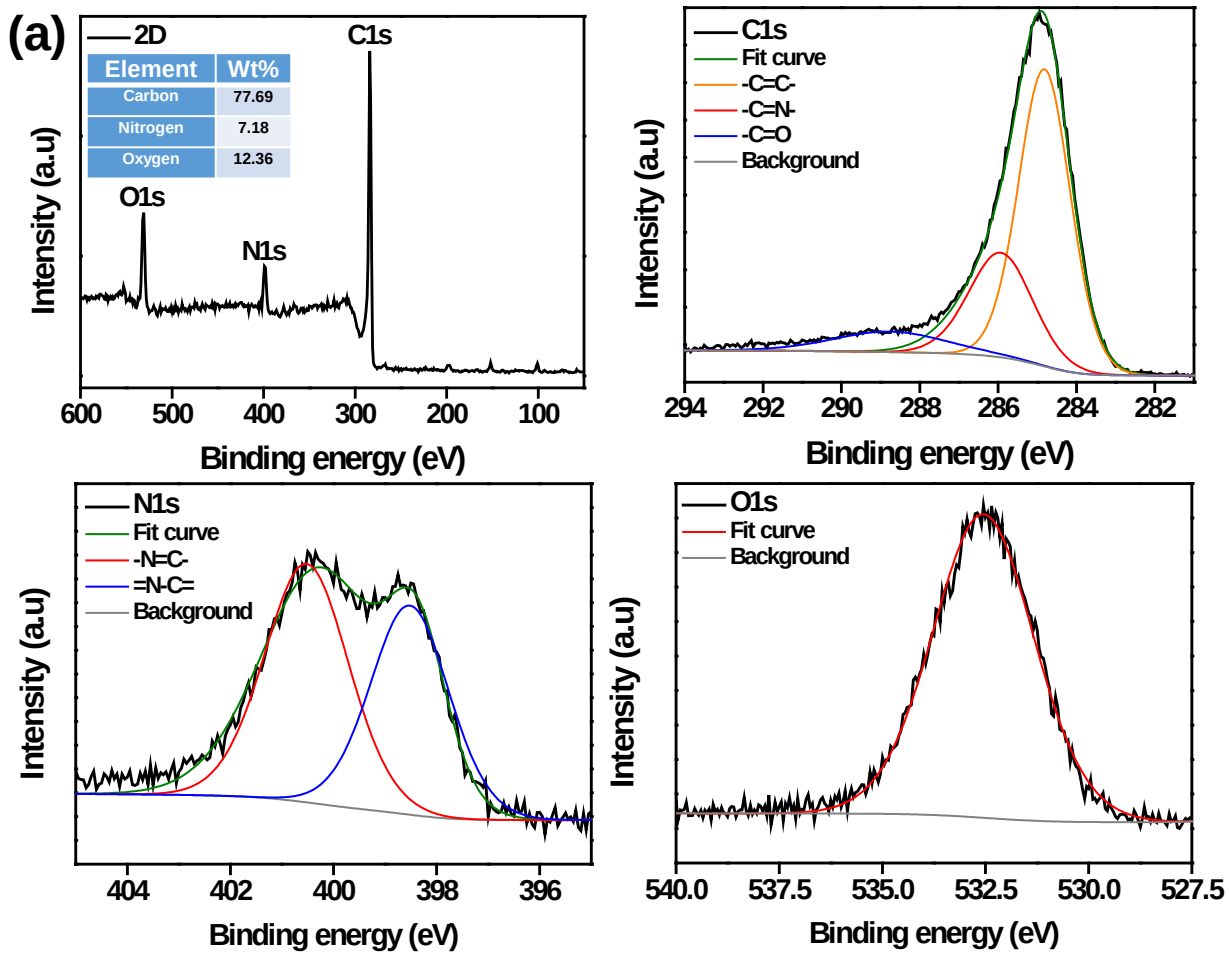

Figure S13. (a) XPS survey, (b) C 1s, (c) N 1s, (d) O 1s spectra of 2D-MGF synthesized at 450^{o}C.

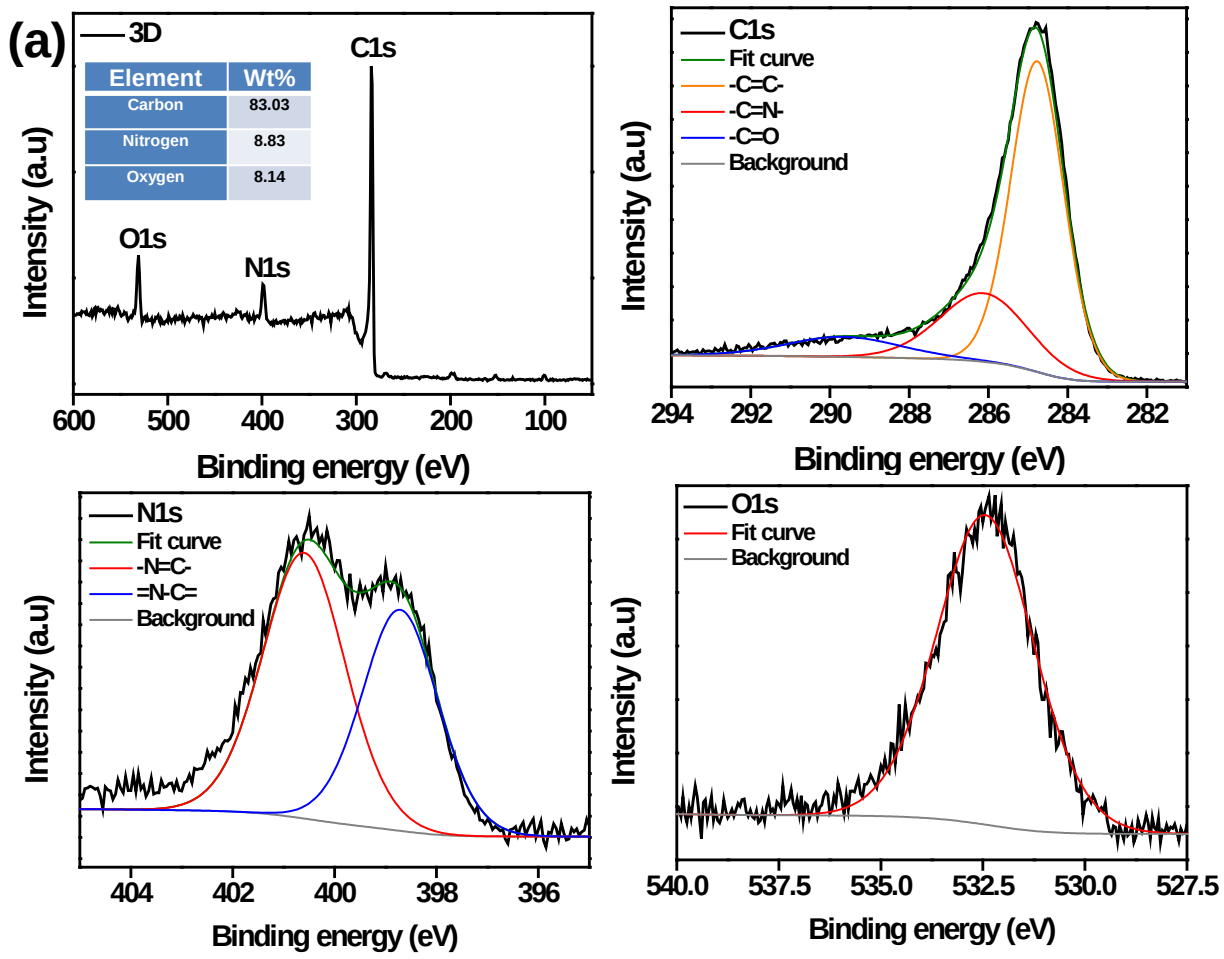

Figure S14. (a) XPS survey, (b) C 1s, (c) N 1s, (d) O 1s spectra of 3D-MGF synthesized at 350°C.

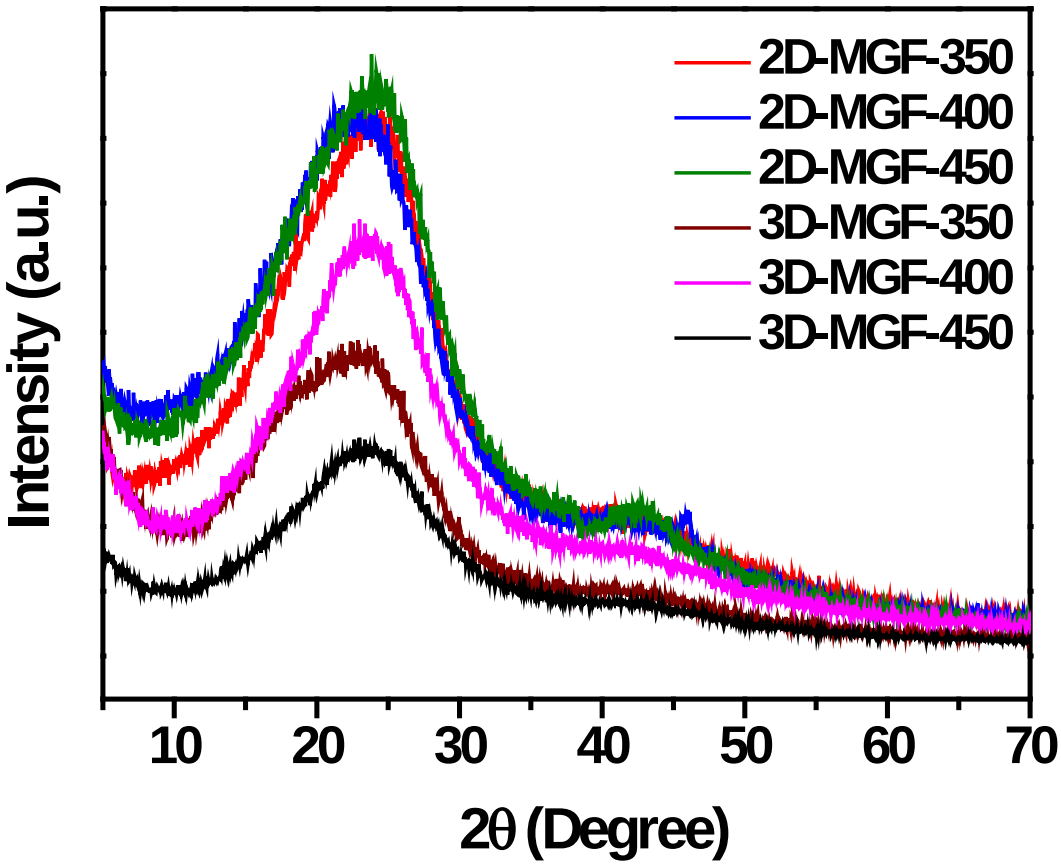

Figure S15. Powder X-ray diffraction (PXRD) profiles of 2D and 3D-MGFs in the 2Θ range of 5 to 70^{o}, indicating amorphous nature of resulting frameworks.

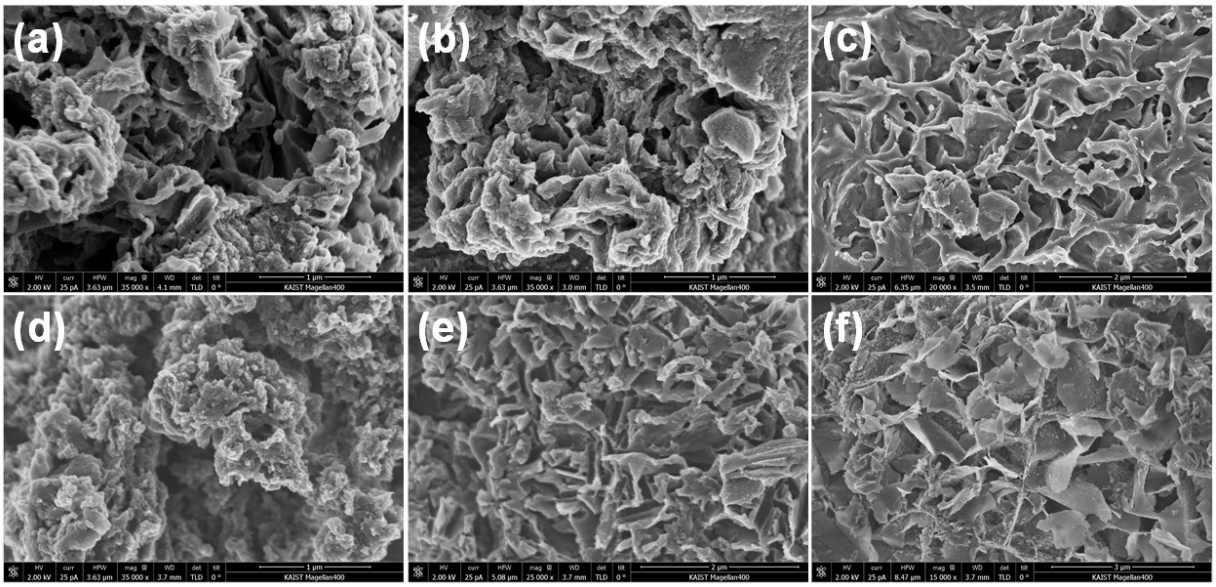

Figure S16. FE-SEM images of 2D and 3D-MGFs synthesized at various temperatures (a) 2D-MGF-350, (b) 2D-MGF-400, (c) 2D-MGF-450, (d) 3D-MGF-350, (e) 3D-MGF-400 and (f) 3D-MGF-450. These results clearly demonstrate graphitization with raising reaction temperature.

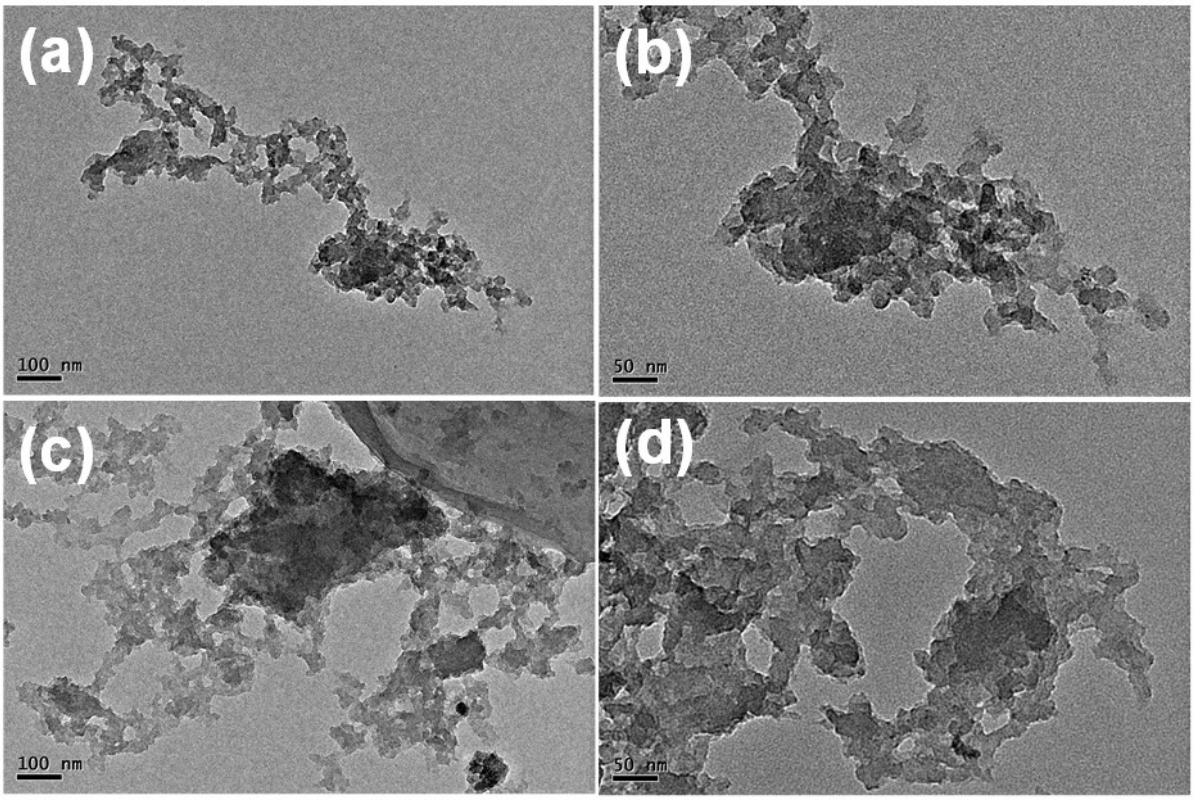

Figure S17. TEM images of (a-b) 2D-MGF-450 and (c-d) 3D-MGF-350.

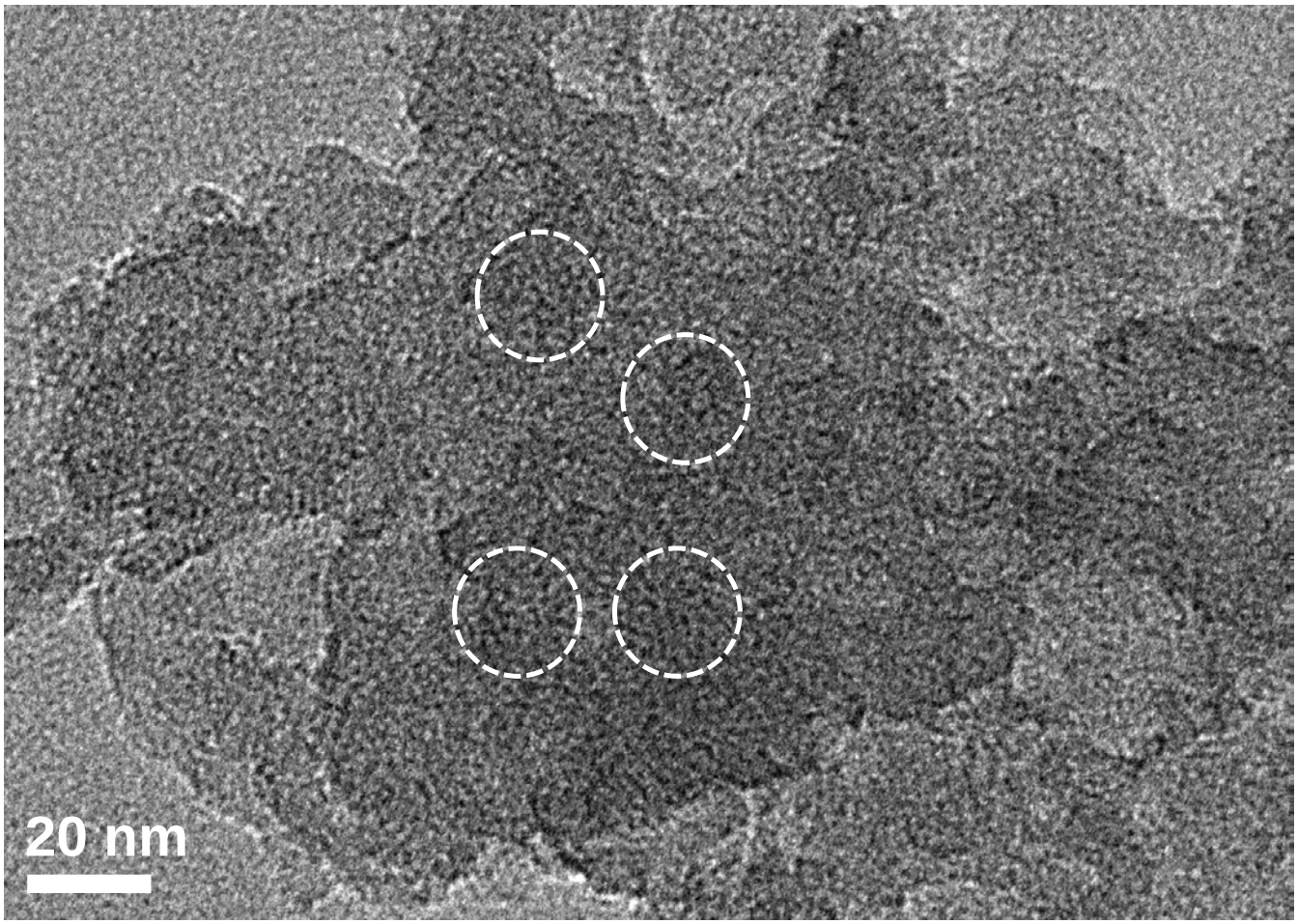

Figure S18. HRTEM image and pore markings of 2D-MGF-450.

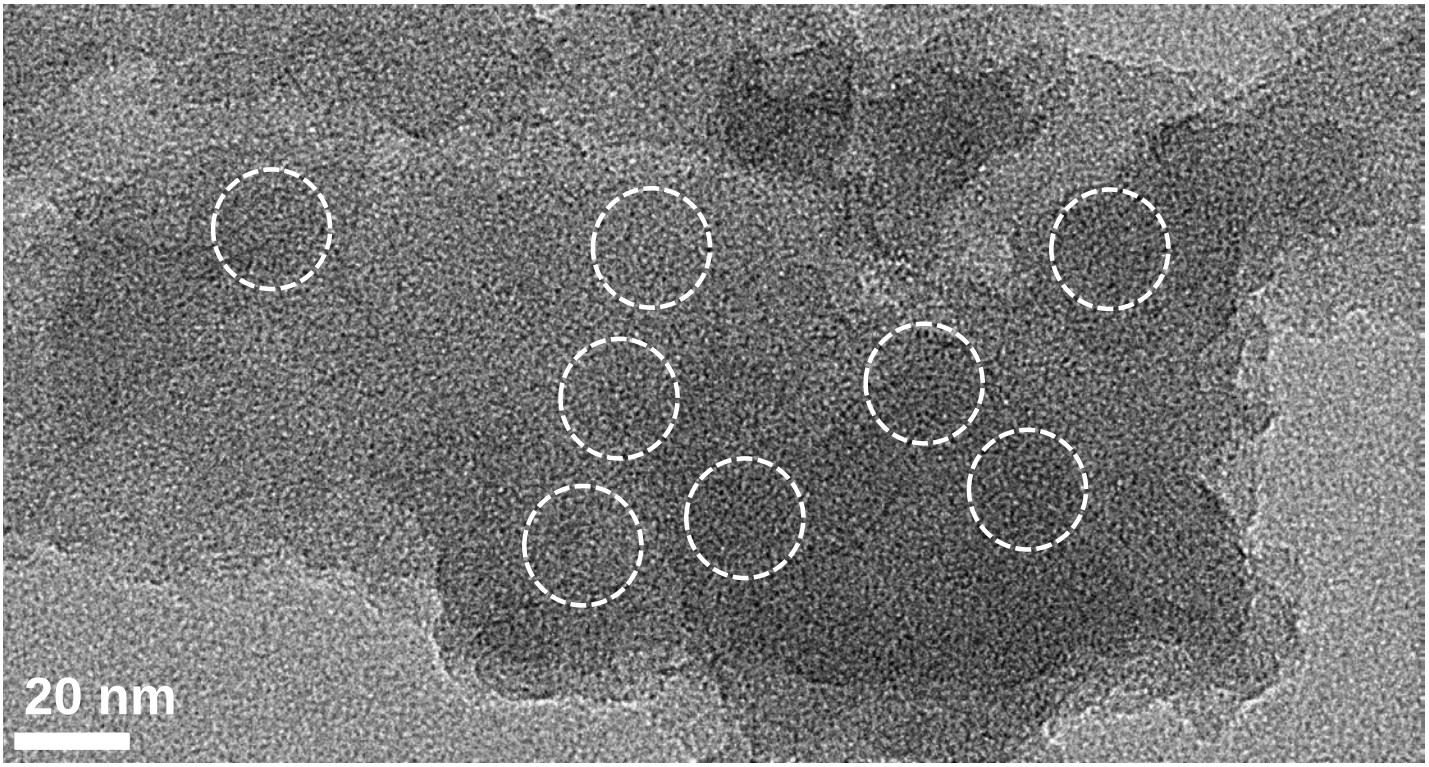

Figure S19. HRTEM image and pore markings of 3D-MGF-350.

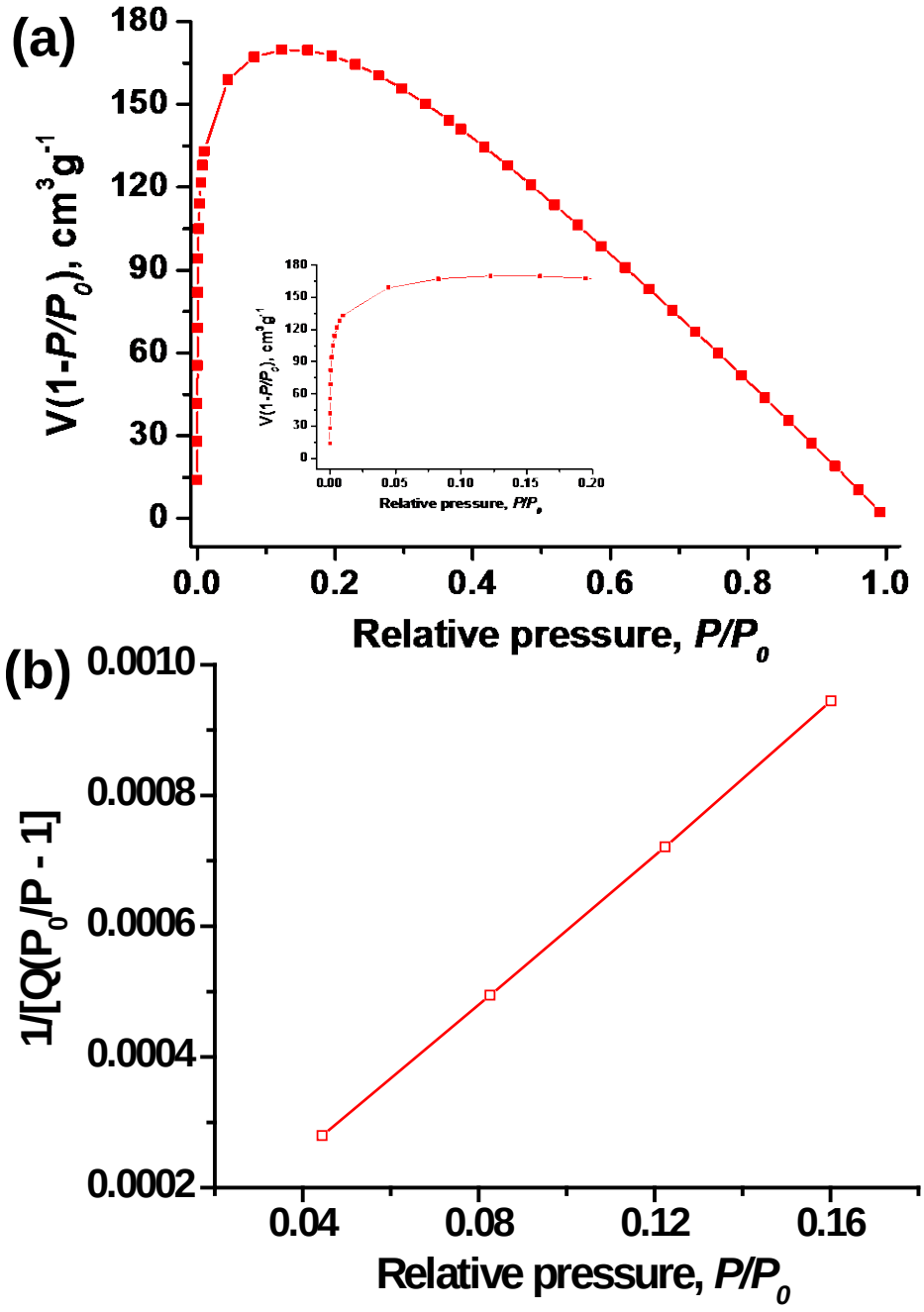

Figure S20. (a) Calculated Rouquerol plot for 2D-MGF-350 (Inset: enlarged plot) along with the pressure ranges used for the BET surface area calculations. We have used the pressure range where the term $V(1-P/P_0)$ continuously increases with P/P_0 for the surface area calculations; **(b)** BET plot of 2D-MGF-350 obtained from argon isotherms at 87 K. The selected points are located in the pressure ranges of 0.01 to 0.16 according to the Rouquerol plots.

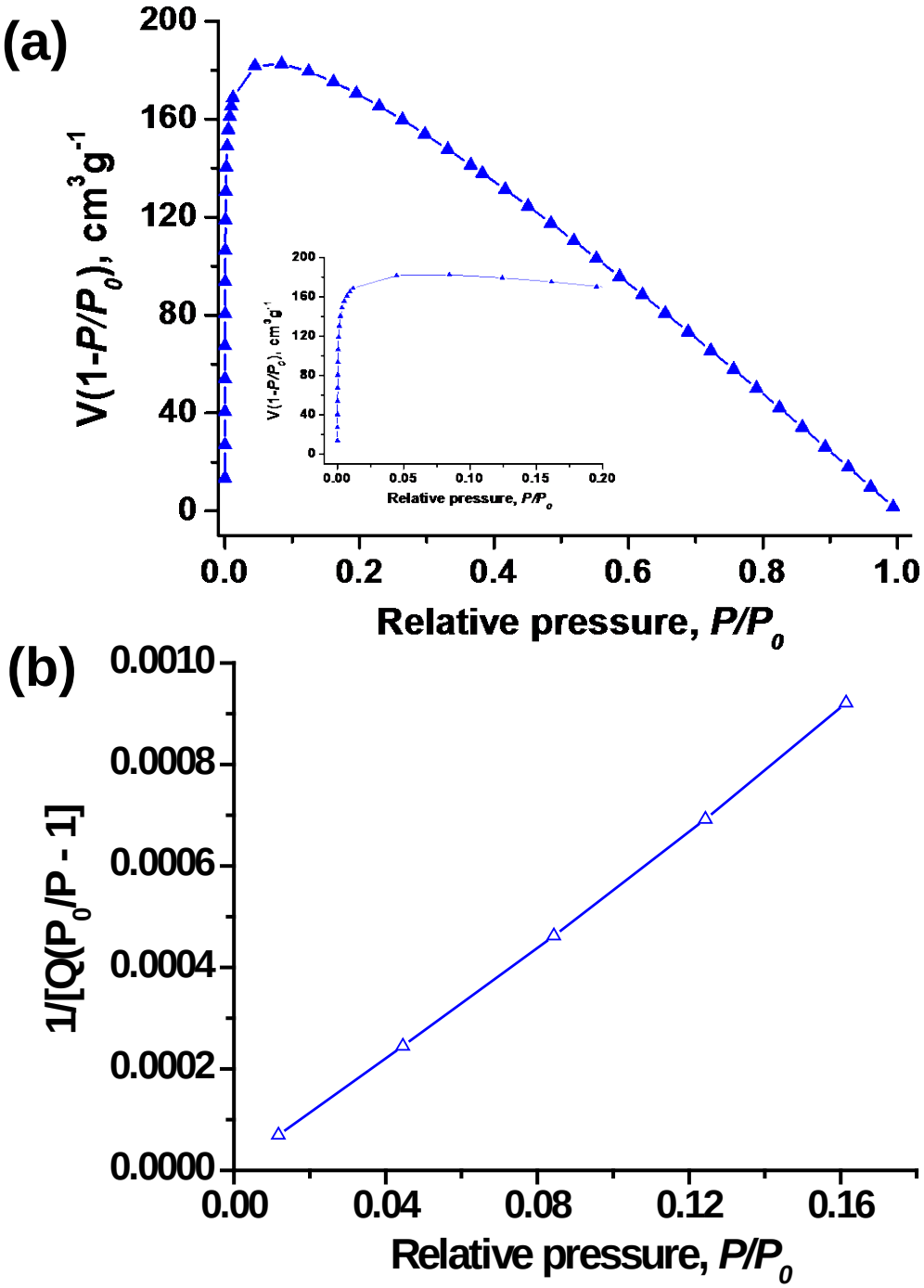

Figure S21. (a) Calculated Rouquerol plot for 2D-MGF-400 (Inset: enlarged plot) along with the pressure ranges used for the BET surface area calculations. We have used the pressure range where the term $V(1-P/P_0)$ continuously increases with P/P_0 for the surface area calculations; **(b)** BET plot of 2D-MGF-400 obtained from argon isotherms at 87 K. The selected points are located in the pressure ranges of 0.01 to 0.16 according to the Rouquerol plots.

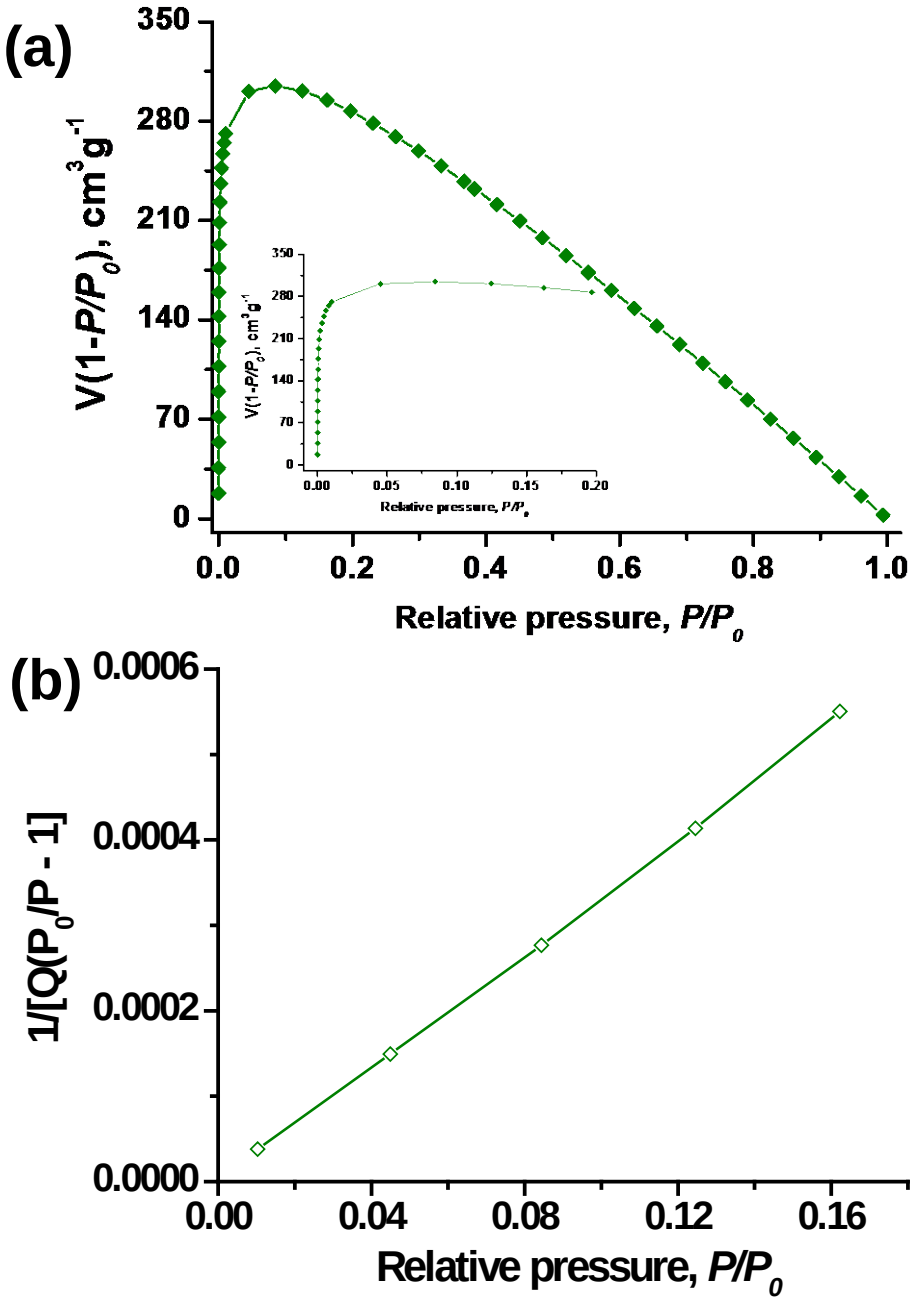

Figure S22. (a) Calculated Rouquerol plot for 2D-MGF-450 (Inset: enlarged plot) along with the pressure ranges used for the BET surface area calculations. We have used the pressure range where the term $V(1-P/P_0)$ continuously increases with P/P_0 for the surface area calculations; **(b)** BET plot of 2D-MGF-450 obtained from argon isotherms at 87 K. The selected points are located in the pressure ranges of 0.01 to 0.16 according to the Rouquerol plots.

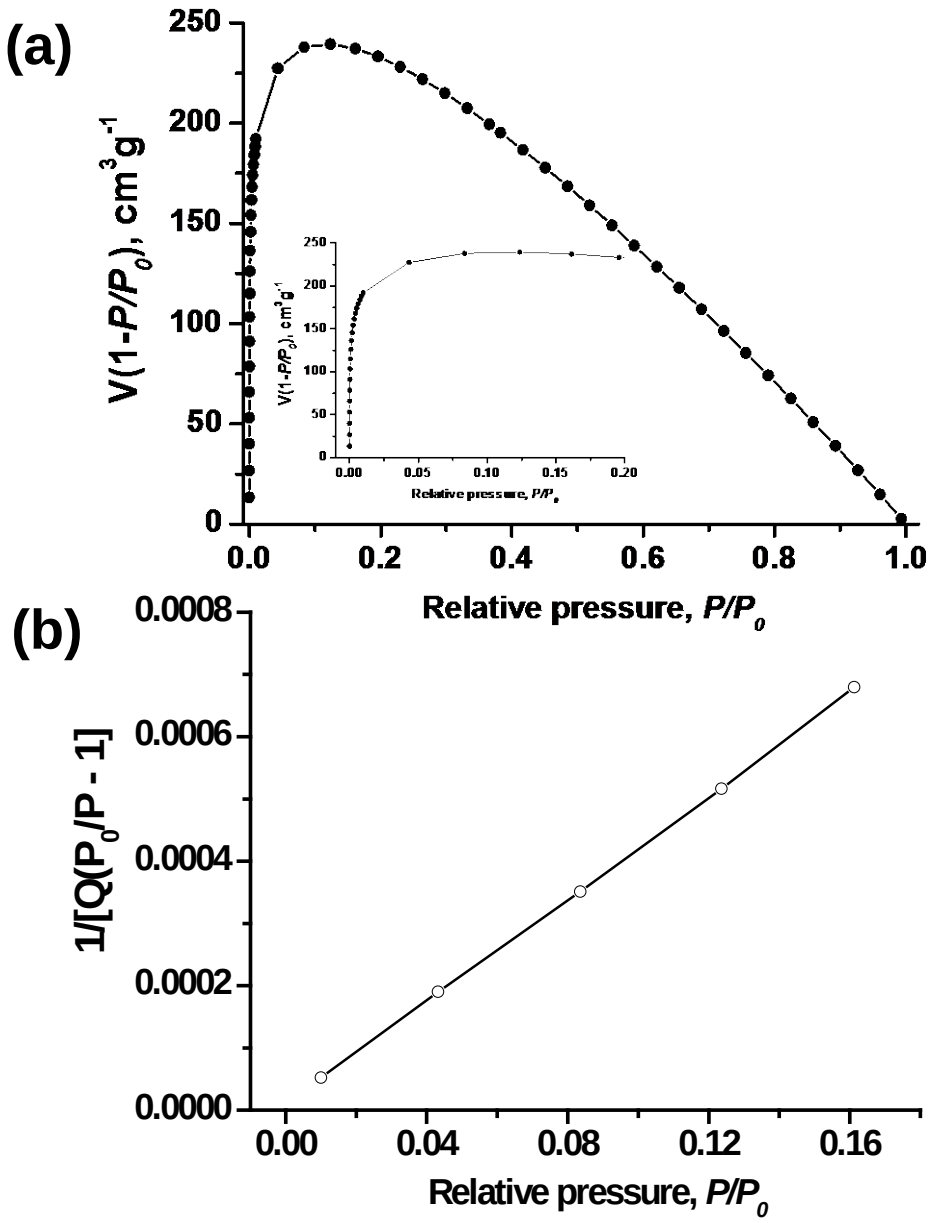

Figure S23. (a) Calculated Rouquerol plot for 3D-MGF-350 (Inset: enlarged plot) along with the pressure ranges used for the BET surface area calculations. We have used the pressure range where the term $V(1-P/P_0)$ continuously increases with P/P_0 for the surface area calculations; **(b)** BET plot of 3D-MGF-350 obtained from argon isotherms at 87 K. The selected points are located in the pressure ranges of 0.01 to 0.16 according to the Rouquerol plots.

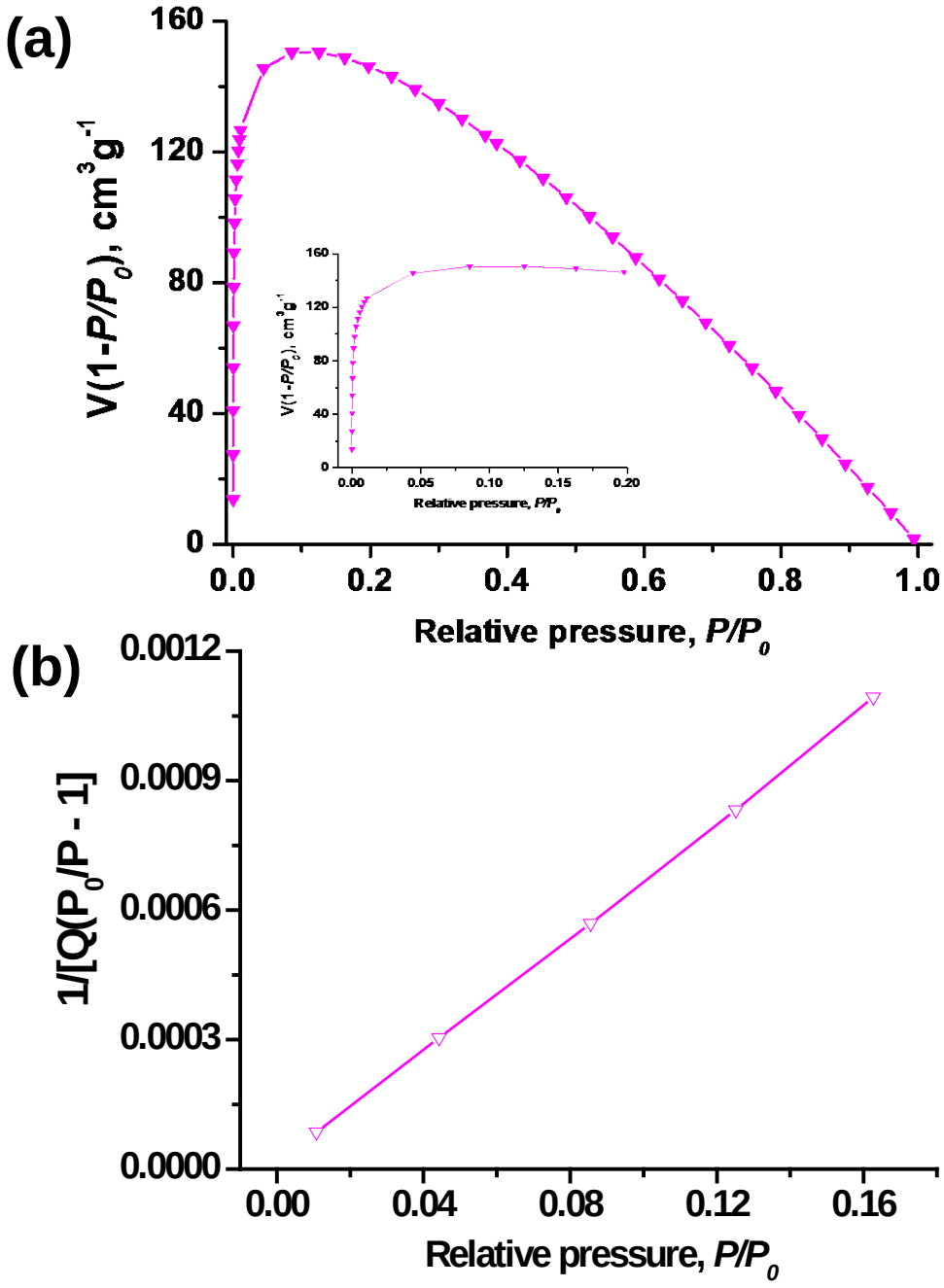

Figure S24. (a) Calculated Rouquerol plot for 3D-MGF-400 (Inset: enlarged plot) along with the pressure ranges used for the BET surface area calculations. We have used the pressure range where the term $V(1-P/P_0)$ continuously increases with P/P_0 for the surface area calculations; **(b)** BET plot of 3D-MGF-400 obtained from argon isotherms at 87 K. The selected points are located in the pressure ranges of 0.01 to 0.16 according to the Rouquerol plots.

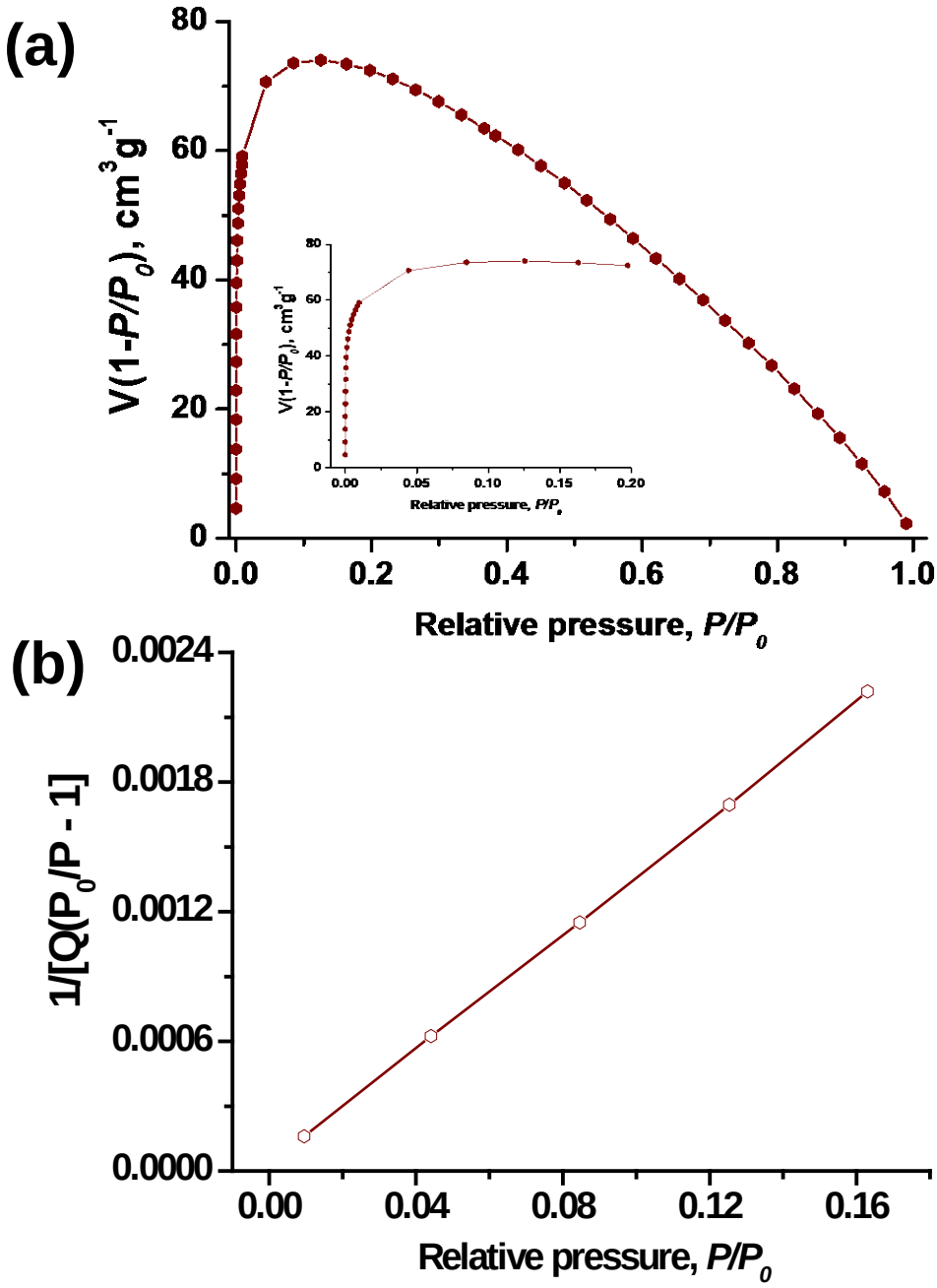

Figure S25. (a) Calculated Rouquerol plot for 3D-MGF-450 (Inset: enlarged plot) along with the pressure ranges used for the BET surface area calculations. We have used the pressure range where the term $V(1-P/P_0)$ continuously increases with P/P_0 for the surface area calculations; **(b)** BET plot of 3D-MGF-450 obtained from argon isotherms at 87 K. The selected points are located in the pressure ranges of 0.01 to 0.16 according to the Rouquerol plots.

Table S1. Textural properties including surface areas and corresponding pore volumes of MGFs and their elemental analysis

Sample	S_{BET}[a] (m^2g^{-1})	Langmuir (m^2g^{-1})	V_{micro}[b] (cm^3g^{-1})	d_{micro}[c] (nm)	S_{ext} (m^2g^{-1})	S_{micro}[d] (m^2g^{-1})	V_{total}[e] (cm^3g^{-1})	I_D/I_G[f]	Elemental analysis (wt.%)		
									C	N	H
2D-MGF-350	666	819	0.11	0.61	322	344	0.34	0.83	76.5	9.7	3.72
2D-MGF-400	677	823	0.19	0.57	505	172	0.36	0.88	77.2	7.7	3.45
2D-MGF-450	1143	1387	0.30	0.60	341	802	0.60	0.95	75.8	8.3	2.79
3D-MGF-350	928	1135	0.19	0.57	406	522	0.49	0.94	82.7	9.3	3.3
3D-MGF-400	580	714	0.118	0.61	320	260	0.306	0.96	81.9	8.5	3.1
3D-MGF-450	287	354	0.051	0.54	141	146	0.19	1.01	80.8	8.3	2.9

[a] Brunauer–Emmett–Teller (BET) surface areas were calculated over the pressure range (P/P_0) 0.01–0.16. [b] Micropore volume calculated using the *t*-plot method. [c] Micropore diameter calculated from NLDFT method. [d] Micropore surface area calculated from the adsorption isotherms using the *t*-plot method. [e] Total pore volume obtained at $P/P_0 = 0.99$. [f] I_D/I_G values were derived from Raman spectra.

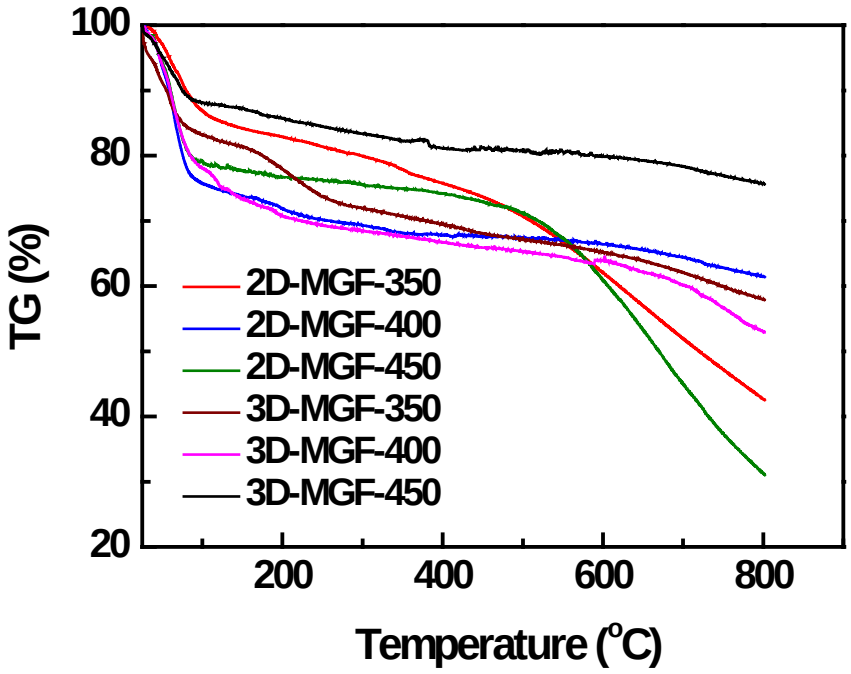

Figure S26. Thermogravimetric analysis (TGA) profiles of 2D- and 3D-MGFs in the temperature range of 25 to 800°C under the N_2 atmosphere.

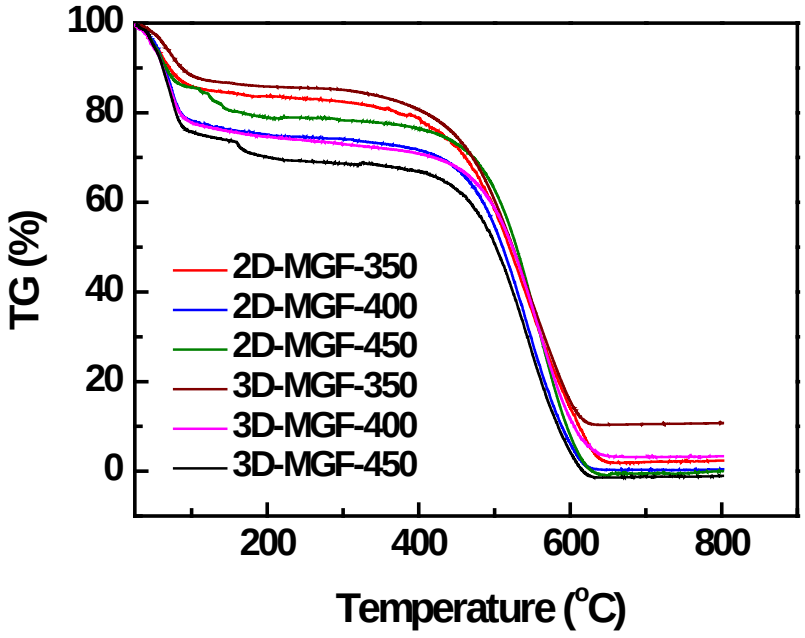

Figure S27. Thermogravimetric analysis (TGA) profiles of 2D- and 3D-MGFs in the temperature range of 25 to 800°C under air atmosphere.

6. Electrochemical characterization of 2D and 3D-MGFs

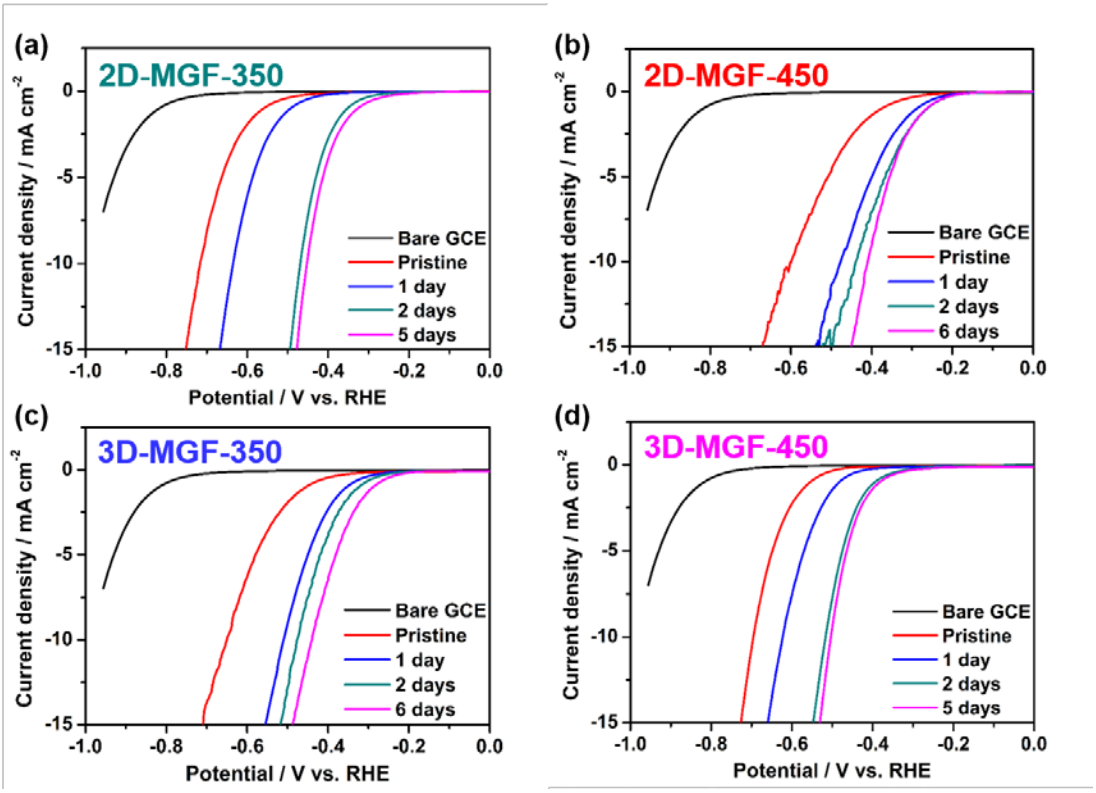

Figure S28. Polarization curves (after iR-correction) of (a) 2D-MGF-350, (b) 2D-MGF-450, (c) 3D-MGF-350, and (d) 3D-MGF-450, which were immersed in 0.5 M H_2SO_4, as a function of immersion periods: Pristine (i.e., As-prepared state), 1 day, 2 days, and 6 days except 2D-MGF-350 and 3D-MGF-450 which were found to saturate after 5 days.

Table S2. Electrochemical HER performance of H^+-2D-MGF-450 and H^+-3D-MGF-350 in acidic media (i.e., 0.5 M H_2SO_4), compared with the representative N-doped graphene materials

N-doped Graphene-based Electrocatalysts	**Onset** (mV)	**$\eta_{-10\ mA\ cm^{-2}}$** (mV)	**Tafel slope** ($mV\ dec^{-1}$)	**Ref.**
N-graphene	-400	~550	~100	[9]
N-doped graphene	-330	490	116	[10]
N-doped nanoporous graphene (N-pGr)	-242	484	129	[11]
N-doped 3D nanoporous graphene (N500)	-320	474	172	[12]
H^+-3D-MGF-350	**-260**	**440**	**121**	**This work**
H^+-2D-MGF-450	**-230**	**410**	**110**	**This work**

7. References

1. A.-S. Castanet, F. Colobert and P.-E. Broutin, *Tetrahedron Lett.*, 2002, **43**, 5047-5048.
2. A. Fürstner and J. W. J. Kennedy, *Chem. Eur. J.*, 2006, **12**, 7398-7410.
3. H. Tohma, H. Morioka, S. Takizawa, M. Arisawa and Y. Kita, *Tetrahedron*, 2001, **57**, 345-352.
4. M. J. Niphakis, B. C. Gay, K. H. Hong, N. P. Bleeker and G. I. Georg, *Bioorg. Med. Chem.*, 2012, **20**, 5893-5900.
5. S. M. H. Kabir and M. Iyoda, *Synthesis*, 2000, 1839-1842.
6. X. Xiong, C.-L. Deng, B. F. Minaev, G. V. Baryshnikov, X.-S. Peng and H. N. C. Wong, *Chem. Asian J.*, 2015, **10**, 969-975.
7. C. Hägele, E. Wuckert, S. Laschat and F. Giesselmann, *ChemPhysChem*, 2009, **10**, 1291-1298.
8. R. Zniber, R. Achour, M. Z. Cherkaoui, B. Donnio, L. Gehringer and D. Guillon, *J. Mater. Chem.*, 2002, **12**, 2208-2213.
9. Y. Zheng, Y. Jiao, Y. Zhu, L. H. Li, Y. Han, Y. Chen, A. Du, M. Jaroniec and S. Z. Qiao, *Nat. Commun.*, 2014, **5**.
10. Y. Zheng, Y. Jiao, L. H. Li, T. Xing, Y. Chen, M. Jaroniec and S. Z. Qiao, *ACS Nano*, 2014, **8**, 5290-5296.
11. S. S. Shinde, A. Sami and J.-H. Lee, *ChemCatChem*, 2015, **7**, 3873-3880.
12. Y. Ito, W. Cong, T. Fujita, Z. Tang and M. Chen, *Angew. Chem. Int. Ed.*, 2015, **54**, 2131-2136.